LJMU Research Online

Fragkoudi, F, Grand, RJJ, Pakmor, R, Gómez, F, Marinacci, F and Springel, V

 Bar formation and evolution in the cosmological context: Inputs from the Auriga simulations

http://researchonline.ljmu.ac.uk/id/eprint/26177/

Article

For more information please contact researchonline@ljmu.ac.uk

Bar formation and evolution in the cosmological context: inputs from the Auriga simulations

Francesca Fragkoudi [1]★ Robert J. J. Grand [2] Rüdiger Pakmor [3] Facundo Gómez [4,5]
Federico Marinacci [6] and Volker Springel[3]

[1]*Institute for Computational Cosmology, Department of Physics, Durham University, South Road, Durham DH1 3LE, UK*
[2]*Astrophysics Research Institute, Liverpool John Moores University, 146 Brownlow Hill, Liverpool L3 5RF, UK*
[3]*Max-Planck-Institut für Astrophysik, Karl-Schwarzschild-Str. 1, D-85748 Garching, Germany*
[4]*Instituto de Investigación Multidisciplinar en Ciencia y Tecnología, Universidad de La Serena, Raúl Bitrán 1305, La Serena, Chile*
[5]*Departamento de Astronomía, Universidad de La Serena, Av. Juan Cisternas 1200 Norte, La Serena, Chile*
[6]*Department of Physics & Astronomy 'Augusto Righi', University of Bologna, via Gobetti 93/2, I-40129 Bologna, Italy*

ABSTRACT

Galactic bars drive the internal evolution of spiral galaxies, while their formation is tightly coupled to the properties of their host galaxy and dark matter halo. To explore what drives bar formation in the cosmological context and how these structures evolve throughout cosmic history, we use the Auriga suite of magneto-hydrodynamical cosmological zoom-in simulations. We find that bars are robust and long-lived structures, and we recover a decreasing bar fraction with increasing redshift which plateaus around ~ 20 per cent at $z \sim 3$. We find that bars which form at low and intermediate redshifts grow longer with time, while bars that form at high redshifts are born 'saturated' in length, likely due to their merger-induced formation pathway. This leads to a larger bar-to-disc size ratio at high redshifts as compared to the local Universe. We subsequently examine the multidimensional parameter space thought to drive bar formation. We find that barred galaxies tend to have lower Toomre Q values at the time of their formation, while we do not find a difference in the gas fraction of barred and unbarred populations when controlling for stellar mass. Barred galaxies tend to be more baryon-dominated at all redshifts and assemble their stellar mass earlier, while galaxies that are baryon-dominated but that do not host a bar, have a higher *ex situ* bulge fraction. We explore the implications of the baryon-dominance of barred galaxies on the Tully–Fisher relation, finding an offset from the unbarred relation; confirming this in observations would serve as additional evidence for dark matter, as this behaviour is not readily explained in modified gravity scenarios.

Key words: methods: numerical – Galaxy: evolution – Galaxy: formation – galaxies: bar – galaxies: kinematics and dynamics.

1 INTRODUCTION

The question of why some galaxies form a stellar bar and others do not has puzzled astronomers for over a century now. Since the early studies on the morphology of 'extra-galactic nebulae', Curtis (1918) noted that some spiral galaxies have 'a band of matter extending diametrically across the nucleus and inner parts of the spiral', which he dubbed the 'ϕ-type spirals', due to their rough similarity to the Greek letter ϕ. Hubble later classified galaxies into the now commonly used 'Hubble Sequence', separating spiral galaxies into what he called the 'normal' spirals, and the 'barred' spirals (Hubble 1926, 1936). We now know that such barred spirals are in fact as common, if not more so, than unbarred spirals in the local Universe, with some studies finding bar fractions as high as 70 per cent, depending on the wavelength and method used to identify them (Eskridge et al. 2000; Menéndez-Delmestre et al. 2007; Aguerri,

Méndez-Abreu & Corsini 2009; Gadotti 2009; Masters et al. 2011; Erwin 2018).

While the fraction of barred galaxies is high in the local Universe, it is generally found to decrease towards higher redshifts (Sheth et al. 2008; Melvin et al. 2014; Simmons et al. 2014, but see also Jogee et al. 2004). Studies using data from the *Hubble Space Telescope* find that bars are present in about ~ 10 per cent of disc galaxies up to $z \sim 2$ (e.g. Simmons et al. 2014), while more recent studies using data from JWST find multiple bars at $z > 1$ (e.g. Costantin et al. 2023; Guo et al. 2023) and a higher bar fraction than previously reported: $\sim$20 per cent at $z \sim 1$–2 and $\sim$15 per cent between $z \sim 2$ and 3 (Le Conte et al. 2024). Bars have also recently been identified out to redshifts of $z \sim 4$ (Smail et al. 2023; Tsukui et al. 2024; Amvrosiadis et al. 2025). At the same time, studies exploring stellar populations in local galaxies find evidence of old bars in the local Universe (Gadotti et al. 2015; de Sá-Freitas et al. 2023; de Sà-Freitas et al. submitted), suggesting that these structures are robust and long-lived. The decreasing fraction of bars at higher redshifts hints at that the tight link between bar formation and the evolution of spiral galaxies, while their presence

★ E-mail: francesca.fragkoudi@durham.ac.uk

in the early Universe suggests that spiral galaxies might be more dynamically mature at these early times than previously thought (see also e.g. Rizzo et al. 2020; Lelli et al. 2021).

Bars affect their host galaxy in a variety of ways, and their formation marks a period in which internal evolutionary processes begin to dominate (e.g. Kormendy & Kennicutt 2004). As they evolve, bars are found to grow longer with time (e.g. Athanassoula & Misiriotis 2002; Ghosh & Di Matteo 2024), due to their ability to exchange angular momentum in the galaxy (Lynden-Bell & Kalnajs 1972), i.e. by emitting angular momentum from material at resonance in the inner disc, which is then absorbed by resonant material in the outer disc and the spheroidal halo (Sellwood 1980; Athanassoula 2002). Bars affect the galaxy's evolution by funnelling gas within the bar to the central-most regions of the galaxy, where it can form nuclear structures such as nuclear discs and rings (e.g. Athanassoula 1992; Knapen, Pérez-Ramírez & Laine 2002; Comerón et al. 2010; Ellison et al. 2011; Fragkoudi, Athanassoula & Bosma 2016; Sormani et al. 2018; de Lorenzo-Cáceres et al. 2019; Gadotti et al. 2019; Leaman et al. 2019; Méndez-Abreu et al. 2019; Bittner et al. 2020). They also re-shape the inner regions of their host galaxies via the formation of a vertically extended bulge, referred to as an X-shaped or boxy/peanut (b/p) bulge, which forms due to vertical instabilities in the bar, is supported by resonant orbits (Combes et al. 1990; Pfenniger & Friedli 1991; Raha et al. 1991; Patsis, Skokos & Athanassoula 2002; Martinez-Valpuesta, Shlosman & Heller 2006; Quillen et al. 2014; Fragkoudi et al. 2015; Portail, Wegg & Gerhard 2015; Sellwood & Gerhard 2020; Li et al. 2023), and which redistributes stars and gas in the inner regions (e.g. Ness et al. 2013; Di Matteo et al. 2015; Fragkoudi et al. 2017b, c, 2018; Debattista et al. 2020).

There are a number of properties which are known to be important in determining whether a bar can form or not, and which determine how it subsequently evolves. For example, an axisymmetric stellar disc will be unstable to local instabilities if it is too 'cold', i.e. if it does not have any *random motions* (Toomre 1964). The early work of Hohl (1971) explored the long-term stability of stellar discs using *N*-body simulations to establish that even when a disc has enough velocity dispersion to prevent axisymmetric instabilities (i.e. when the Toomre stability criterion $Q > 1$), it can still be unstable to global bar-forming modes. Subsequent work has shown that further increasing the velocity dispersion of a disc can delay bar formation, and lead to an overall weaker bar, but might not be enough to completely stabilize the disc against bar formation (e.g. Athanassoula & Sellwood 1986; Combes et al. 1990).

Another fundamental parameter which sets whether a galaxy will form a bar, is its *disc-dominance*, i.e. how much the stellar disc dominates over the dark matter halo in the inner regions. In this work, we will interchangeably use either 'disc-dominance' or 'baryon-dominance' to refer to this, as both are used in the literature. Ostriker & Peebles (1973) showed that embedding an otherwise unstable disc within a massive halo can stabilize it against bar formation; the existence of a large number of unbarred galaxies in the Universe therefore provided an early indication of the existence of such massive haloes surrounding spiral galaxies. The disc dominance of a galaxy is usually defined as the disc's contribution to the circular velocity curve at a given characteristic radius, e.g. at 2.2 disc scale-lengths (Sackett 1997; see also Efstathiou, Lake & Negroponte 1982) – and as such depends on the enclosed mass within that radius. Later works further expanded on the interaction between bars and haloes, such as the seminal paper of Athanassoula (2002), which showed that while dark matter haloes can stabilize the disc against bar formation for an initial period of time, the existence of a *live* dark matter halo in fact helps bars grow longer and stronger later in

their evolution. This occurs because a 'live' halo is able to absorb the angular momentum emitted by the disc via the bar, whereas in the case of a disc embedded within a static halo, only the outer disc is available to act as a 'absorber' of angular momentum. This 'emission' and 'absorption' of angular momentum in the galaxy is driven by the bar, i.e. the inner regions of the disc emit angular momentum – which leads to a longer and stronger bar – while the outer disc and halo absorb the angular momentum, leading to a more extended disc and to an increase in net rotation in the halo. It is important to note that the velocity dispersion of the halo – not just its mass – play a role in the angular momentum transfer (Athanassoula 2003), which further complicates matters.

While the dark matter halo is the most massive 'spheroid' in the galaxy, a *spheroidal bulge component* in the central regions will also contribute to stabilizing the disc against bar formation (Ostriker & Peebles 1973), while also acting as an absorber of angular momentum from the bar (e.g. Saha, Martinez-Valpuesta & Gerhard 2012). The resonant processes driving this redistribution of angular momentum are similar to those taking place between the bar and the halo; the absorption of angular momentum by the bulge/spheroid reduces the angular momentum of the disc and can lead to the spin-up and flattening of an initially non-rotating spheroidal bulge (e.g. Saha et al. 2012; Saha, Gerhard & Martinez-Valpuesta 2016).

Finally, the *gas fraction* of galaxies has long been thought to play a role in the formation and subsequent evolution of bars. The works of Bournaud & Combes (2002) and Bournaud, Combes & Semelin (2005), which explored bar formation in *N*-body and hydrodynamics simulations, suggested that bars can be weakened or even completely destroyed in the presence of gas. They attributed this to two mechanisms; first, the formation of a central mass concentration (CMC) due to bar-induced gas inflows, which weakens the bar, and second, the transport of angular momentum from the gas to the bar itself. Berentzen et al. (2007) later suggested that the weakening of bars in discs with higher gas fractions is not due to the angular momentum transport between these two components, but rather due to the differences in bar buckling induced by the CMC. CMCs that make up a few per cent of the mass of the stellar disc are thought to contribute to bar weakening and even destruction,[1] and the more concentrated and massive the CMC, the larger this effect (Hasan, Pfenniger & Norman 1993; Norman, Sellwood & Hasan 1996; Athanassoula et al. 2005). Athanassoula, Machado & Rodionov (2013) explored the formation of bars within galaxies with varying gas fractions and haloes of different triaxiality. They found that galaxies that are more gas-rich stay axisymmetric for longer and that once bars start to grow, they do so at a slower rate. Therefore, while gas appears to play a role in bar formation, it is unclear whether this occurs 'directly' due to the exchange of angular momentum between the gas and the bar itself, or whether gas has an 'indirect' effect on bar formation, for example through the formation of a CMC which forms when gas is pushed to the centre by the bar.

The aforementioned studies have largely been carried out using isolated *N*-body simulations. These lend themselves to exploring the internal evolution of galaxies, due to the higher resolution they offer, while they also enable one to isolate specific physical properties to study. However, it is becoming increasingly clear that the mechanisms responsible for bar formation and evolution cannot be decoupled from the cosmological context, since processes such as

---

[1]It is worth noting that the masses and compactness of the CMCs required to completely destroy bars are not readily found in nature (see e.g. the discussion in Athanassoula, Lambert & Dehnen 2005).

mergers (e.g. Athanassoula, Rodionov & Prantzos 2017), interactions (e.g. Łokas 2019), external gas accretion (e.g. Bournaud & Combes 2002), the physics of star formation, and various feedback processes (e.g. Irodotou et al. 2022), as well as the assembly and properties of the dark matter haloes themselves (e.g. Collier, Shlosman & Heller 2018), all play a role in the formation and evolution of bars. Recent advances in terms of numerical resolution and modelling of the physics of baryons have made it possible to begin to use cosmological simulations to explore the internal dynamical evolution of galaxies both in 'zoom-in simulations' (e.g. Kraljic, Bournaud & Martig 2012; Scannapieco & Athanassoula 2012; Buck et al. 2018; Gargiulo et al. 2019; Fragkoudi et al. 2020, 2021; Merrow et al. 2024) as well as in 'large box' cosmological simulations (e.g. Algorry et al. 2017; Peschken & Łokas 2019; Rosas-Guevara et al. 2020; Roshan et al. 2021; Frankel et al. 2022; Gargiulo et al. 2022; Izquierdo-Villalba et al. 2022; López et al. 2024). It is worth noting that all these simulations, which use different prescriptions for modelling the Baryonic physics of galaxy formation and evolution, often lead to substantially different predictions for the fraction of bars (e.g. finding very few bars at low redshifts $z \sim 0.25$; Reddish et al. 2022) as well as for their intrinsic properties (e.g. weak and transient bars; Ansar et al. 2025). As the galaxy formation (or 'baryon' physics) models become more advanced, we can use the properties of bars to constrain these models, since bars act as a litmus test of whether the dynamics of observed discs are being adequately modelled in cosmological simulations.

In this work, we explore the properties of barred galaxies and how these evolve over cosmic history in the Auriga suite of magnetohydrodynamical cosmological zoom-in simulations to provide predictions for the properties of bars in Auriga at both low and high redshifts. We then explore the multidimensional parameter space of bar formation within the cosmological context, by examining the aforementioned parameters thought to be important for bar formation. The paper is structured as follows. In Section 2, we briefly describe the Auriga cosmological simulations, as well as the analysis tools used in this study. In Section 3, we present some of the global properties of barred galaxies in Auriga and show how the length of bars evolves with redshift. In Section 4, we explore the different parameters that affect bar formation, and how these contribute to whether a galaxy will be barred or not in the cosmological context. In Section 5, we discuss some of the implications of our findings on the Tully–Fisher (TF) relation, on bars at high redshift and on the multidimensional parameter space of bar formation. In Section 6, we conclude and summarize our results.

2 THE AURIGA SIMULATIONS

We explore the formation and evolution of bars in the Auriga simulations which are a suite of cosmological magnetohydrodynamical zoom-in simulations of galaxies which span a range of halo masses at $z = 0$ between $M_{200} = 0.5 \times 10^{12} - 2 \times 10^{12} M_\odot$ (Grand et al. 2017, 2019). The simulations are run from redshift $z = 127$ to $z = 0$ with cosmological parameters $\Omega_m = 0.307$, $\Omega_b = 0.048$, and $\Omega_\Lambda = 0.693$, and a Hubble constant of $H_0 = 100h \, \mathrm{km \, s^{-1} \, Mpc^{-1}}$, where $h = 0.6777$ (Planck Collaboration XVI 2014). The simulations are performed with the magnetohydrodynamic code AREPO (Springel 2010; Pakmor et al. 2016), with a comprehensive galaxy formation model (see Vogelsberger et al. 2013; Marinacci, Pakmor & Springel 2014; Grand et al. 2017, for more details) which includes primordial and metal line cooling, a prescription for a uniform background ultraviolet field for reionization (completed at $z = 6$), a subgrid model for star formation, stellar evolution and feedback, magnetic

fields, as well as black hole seeding, accretion, and feedback. The dark matter particles have a mass of $\sim 4 \times 10^5 M_\odot$ and the stars and gas have a mass resolution $\sim 5 \times 10^4 M_\odot$. The physical softening of collisionless particles grows with time and corresponds to a fixed comoving softening length of $500 \, h^{-1}$ pc, while the maximum physical softening allowed is 369 pc (see Power et al. 2003 for a criterion on how to choose softening parameters). The physical softening for the gas cells is scaled by the gas cell radius with a minimum limit of the softening equal to that of the collisionless particles.

Star formation and stellar feedback are modelled as follows: if a given gas cell is eligible for star formation, it is converted (according to the Chabrier 2003 initial mass function) either into a star particle – in which case it represents a single stellar population of a given mass, age and metallicity – or into a site for SNII feedback, i.e. a 'wind' particle. Wind particles are launched in a random direction with a velocity that scales with the 1D local dark matter velocity dispersion (see Grand et al. 2017 for more details). The wind metal content is determined by the initial metallicity of the gas cell from which the wind particle originated, i.e. it is 'loaded' with $\eta = 0.6$ of the total metals of the parent gas cell. For the stellar particles, the mass-loss and metal enrichment from Supernovae Type II and Type Ia (SNII and SNIa) and asymptotic giant branch (AGB) stars is modelled and the mass and metals are distributed among nearby gas cells with a top-hat kernel. We track a total of nine elements: H, He, C, O, N, Ne, Mg, Si, and Fe.

By $z = 0$, the simulations form disc-dominated star-forming galaxies with flat rotation curves that reproduce a range of observed scaling relations such as the TF relation (Grand et al. 2017) and the size–mass relation of H I gas discs (Marinacci et al. 2017). They also form instabilities in the discs such as bars and boxy/peanut bulges (Fragkoudi et al. 2020), which have structural properties (Blázquez-Calero et al. 2020) and pattern speeds (Fragkoudi et al. 2021) in agreement with those of observed bars, and mainly consist of so-called pseudo-bulges (Gargiulo et al. 2019), reproducing what is found for disc galaxies in the local Universe (e.g. Kormendy & Kennicutt 2004; Gadotti 2009).

We note that the full simulation output data for the Auriga simulations has been made publicly available – see Grand et al. (2024) for more details. Various data products on barred galaxies in Auriga, collected in this paper, are now also available with the public data release.[2]

2.1 Barred galaxy sample

In this work, we focus on the galaxies which at $z = 0$ have halo masses in the range of $M_{200} = 0.5 \times 10^{12} - 2 \times 10^{12} M_\odot$. This includes the 30 original Auriga haloes presented in Grand et al. (2017) (Au1-Au30), as well as the 10 slightly lower mass galaxies, first presented in Grand et al. (2019) (Au31-Au40). We exclude Au34 from all the analysis that follows as it has a low-resolution dark matter particle within its virial radius.

In what follows we focus most of the analysis on the barred galaxies in the sample, which can be seen in Fig. 1. We determine whether a galaxy is barred by examining the bar strength, A_2, which we define as the $m = 2$ Fourier mode of the stellar surface density at $z = 0$ (see the next subsection for more details on how the bar strength is obtained). Our 'barred' sample includes all the galaxies which at $z = 0$ have $A_2 \geq 0.25$. This

---

[2]The data can be found at https://wwwmpa.mpa-garching.mpg.de/auriga/.
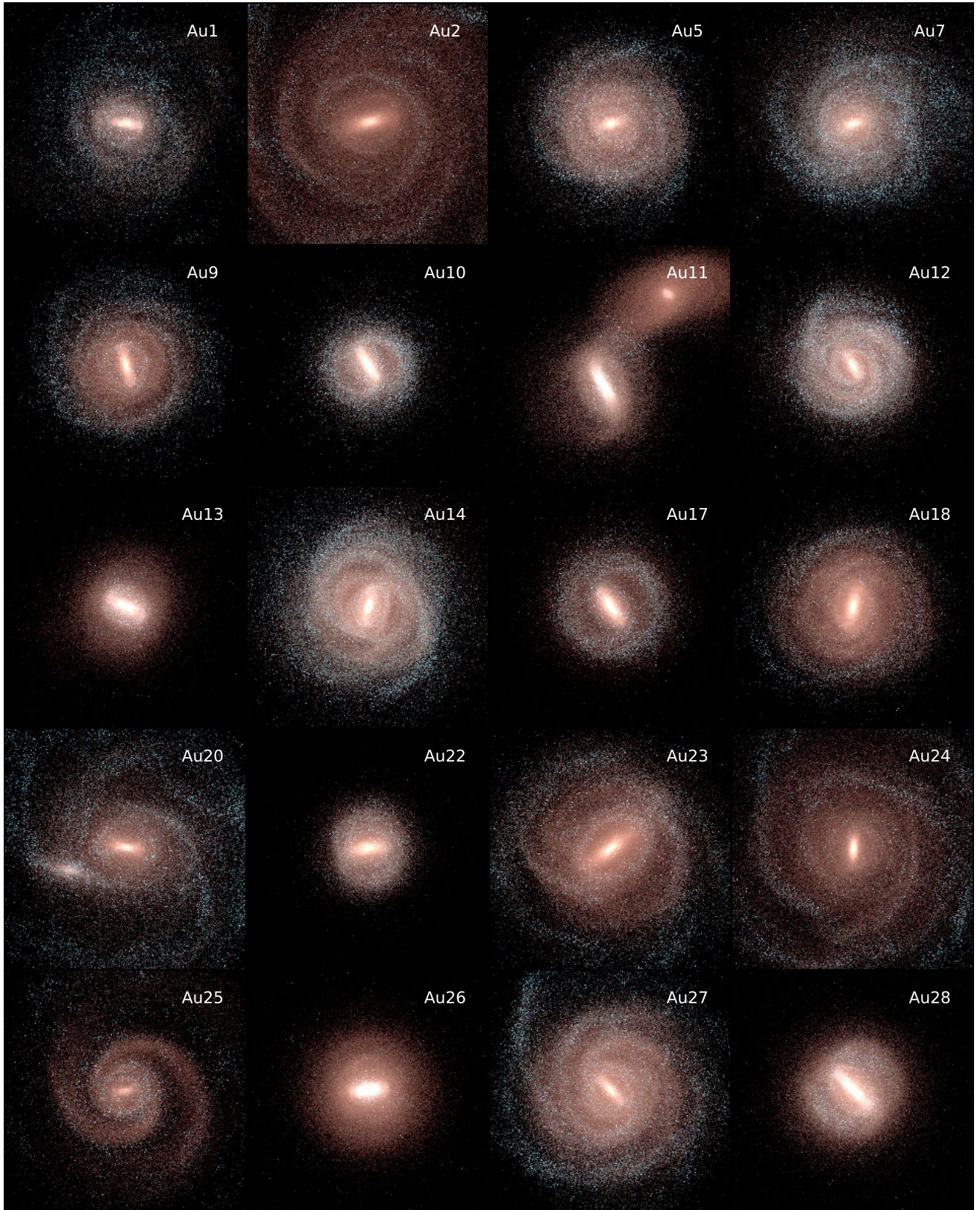
Figure 1. Face-on RGB stellar light projections of the barred galaxies in the Auriga simulations at $z = 0$. The panels have a size of $50\,\mathrm{kpc} \times 50\,\mathrm{kpc}$.
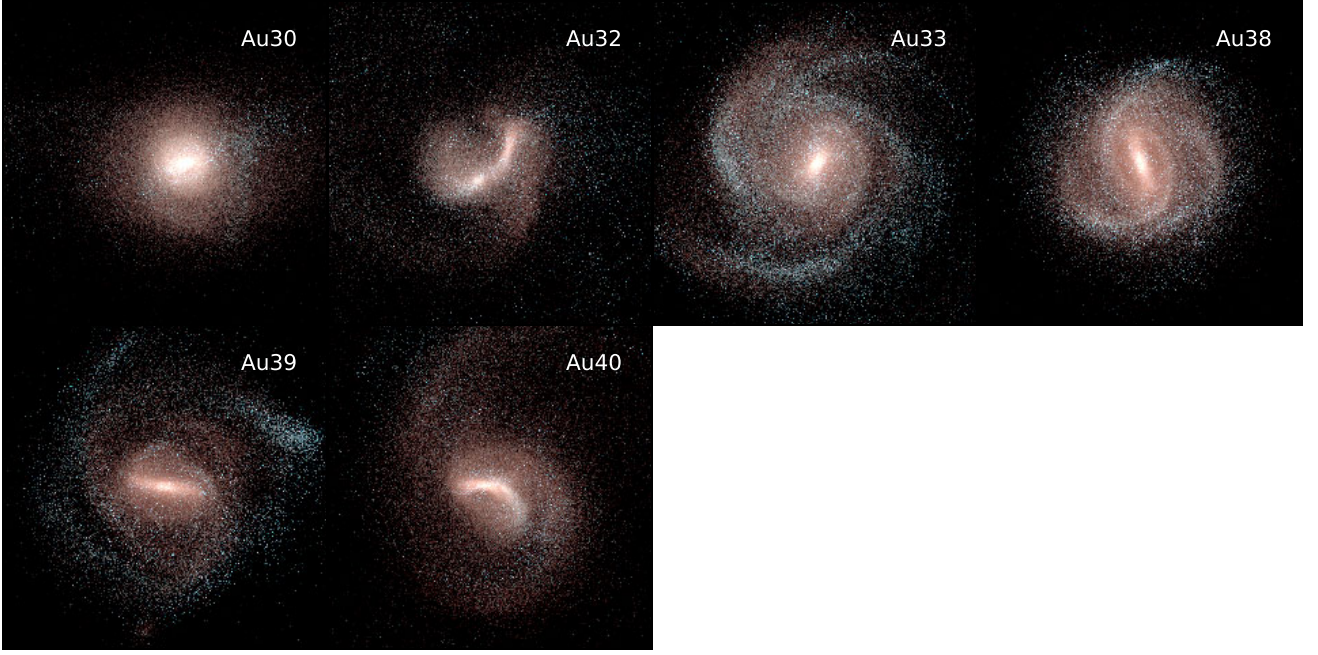
Figure 1. Continued.

results in 26 out of the 39 haloes explored here. The other 13 galaxies are classified as the unbarred sample. For parts of the analysis that follow, we further label the galaxies that undergo an interaction at $z \sim 0$ with a companion. These are labelled as 'interacting' galaxies and are identified by visually inspecting for disturbances in the stellar distribution of the galaxies within a lookback time of $t_{lb} = 500 \, \text{Myr}$. These samples are summarized in Table 1 (see column 'Classification') as well as in Fig. 2, where we plot the bar strength A_2 as a function of stellar mass (bottom panel), the bar fraction versus stellar mass (middle panel) and the mass distribution of the three subsamples (unbarred–blue, barred without interacting–red, and barred including interacting–dashed brown).

2.2 Analysis

Here we describe how we obtain the bar-related parameters for the galaxies in our sample, such as the bar strength, length and bar formation time.

Bar strength, A_2: To obtain the bar strength we first re-align the galaxy, such that the angular momentum vector of the stellar disc is parallel to the z-axis. We then select the stellar particles close to the disc, within a height of $|z| < 0.8 \, \text{kpc}$ above and below the plane. The Fourier modes of the surface density are given by,

$$a_m(R) = \sum_{i=1}^{N} m_i \cos(m\theta_i), \qquad m = 0, 1, 2, ..., \tag{1}$$

$$b_m(R) = \sum_{i=1}^{N} m_i \sin(m\theta_i), \qquad m = 0, 1, 2, ... \tag{2}$$

where m denotes the Fourier mode, m_i is the mass of particle i, R is the cylindrical radius, N is the total number of particles at that radius and θ_i is the azimuthal angle. In order to obtain a single value for the bar strength we take the maximum value of the relative $m = 2$

component within the inner 10 kpc as

$$A_2 = \max \left(\frac{\sqrt{\left(a_2^2(R) + b_2^2(R)\right)}}{a_0(R)} \right). \tag{3}$$

For estimating the bar fraction in Fig. 4 we also visually inspect the galaxies, to ensure that when $A_2 \geq 0.25$, this is not due, for example, to a transient off-centering of the disc due to a merger (which can occur frequently at high redshifts). The aforementioned parameters and cuts used for the bar strength are applied such that our definition of 'barred galaxy' agrees well with tests that were done in which the authors visually identified bars in the simulations. We note that slight changes in these parameters do not change the overall conclusions of this work.

Bar formation time, t_{bf}: In what follows we define the bar formation time t_{bf} as the first lookback time at which A_2 becomes, and subsequently remains, larger than 0.25. In Fig. 3, we show the bar strength A_2 as a function of lookback time, for the barred galaxies in our sample, which we colour-code according to their bar formation time.

Bar length, R_{bar}: There are various methods for estimating the length of the bar, from ellipse-fitting methods used widely in observational studies, to methods using the $m = 2$ Fourier mode of the surface density, which are more commonly employed in numerical studies (see e.g. Erwin 2005; Gadotti 2011; Hilmi et al. 2020; Fragkoudi et al. 2021; Petersen, Weinberg & Katz 2024). Here, we use a method that is well-suited for estimating the bar length in an automated way for simulated galaxies, across a large number of snapshots; that is, we use the radius at which A_2 falls below 70 per cent of its maximum value. The bar length at the time of bar formation can vary rapidly, in particular when the bar forms due to an interaction or after a merger. Therefore, when estimating the bar length at the time of formation, we take the average over three snapshots after t_{bf}. We note that we have tested various methods for

Table 1. Properties of barred galaxies: (1) halo name; (2) A_2 the bar strength at $z = 0$ for the 39 galaxies in this sample; (3) the lookback time of bar formation (t_{bf}) in Gyr; (4) The length of the bar at $z = 0$, (5) the length of the bar at the time of bar formation, (6) the size of the disc at $z = 0$, (7) the size of the disc at the time of bar formation, (8) the stellar mass of the galaxy at $z = 0$, (9) the stellar mass of the galaxy at the time of bar formation, (10) classification of the galaxy as barred, unbarred and whether it falls within our definition of interacting at $z = 0$ (int; see the text for more details).

Halo	$A_2(z=0)$	t_{bf} (Gyr)	$R_b(z=0)$ (kpc)	$R_b(z=z_{bf})$ (kpc)	$R_d(z=0)$ (kpc)	$R_d(z=z_{bf})$ (kpc)	$M_\star(z=0)$ ($10^{10}M_\odot$)	$M_\star(z=z_{bf})$ ($10^{10}M_\odot$)	Classification
Au1	0.55	3.97	4.00	3.16	18.38	8.38	2.74	1.63	Bar, int
Au2	0.43	7.29	5.49	6.82	41.88	20.04	7.04	3.55	Bar
Au3	0.11				32.12		7.75		Unbarred
Au4	0.10				20.38		7.09		Unbarred
Au5	0.35	2.17	3.84	2.62	20.62	18.04	6.72	6.02	Bar
Au6	0.20				27.62		4.75		Unbarred
Au7	0.29	1.66	3.77	1.92	22.38	20.88	4.87	3.68	Bar
Au8	0.18				27.88		2.99		Unbarred
Au9	0.56	6.50	5.92	1.97	19.38	11.79	6.10	3.76	Bar
Au10	0.60	6.17	4.88	4.85	14.88	10.29	5.94	2.85	Bar
Au11	0.52	4.91	4.95	2.68	20.38	15.21	5.56	2.66	Bar, int
Au12	0.38	2.67	3.05	2.51	18.88	18.38	6.01	4.39	Bar
Au13	0.38	3.45	1.73	1.65	15.62	15.04	6.19	4.38	Bar
Au14	0.37	1.47	4.37	2.74	22.38	19.71	10.4	8.98	Bar
Au15	0.10				23.12		3.93		Unbarred
Au16	0.10				36.88		5.41		Unbarred
Au17	0.55	10.37	6.37	5.24	19.12	11.54	7.61	1.68	Bar
Au18	0.38	9.16	5.33	3.81	20.88	12.38	8.04	2.35	Bar
Au19	0.08				25.88		5.32		Unbarred
Au20	0.49	6.68	6.88	2.80	28.38	15.88	4.63	2.01	Bar, int
Au21	0.22				24.38		7.72		Unbarred
Au22	0.43	8.09	5.37	5.88	13.62	11.04	6.02	2.70	Bar
Au23	0.42	5.06	8.46	3.64	26.12	16.96	9.02	6.27	Bar
Au24	0.63	8.53	4.76	5.00	31.62	13.21	6.55	2.65	Bar
Au25	0.28	0.34	1.77	2.67	26.12	25.12	3.14	3.08	Bar, int
Au26	0.46	5.38	4.53	3.80	19.12	15.46	11.0	6.55	Bar
Au27	0.42	2.97	4.96	3.15	24.62	20.62	9.61	8.21	Bar
Au28	0.51	2.79	6.32	4.37	18.12	15.88	10.4	8.80	Bar
Au29	0.19				18.62		9.03		Unbarred
Au30	0.48	0.81	4.60	4.11	18.62	19.38	4.25	3.86	Bar, int
Au31	0.13				19.88		1.80		Unbarred, int
Au32	0.54	3.15	4.70	3.27	18.88	21.12	2.12	1.24	Bar, int
Au33	0.35	1.14	4.70	6.34	23.12	19.21	4.50	3.16	Bar, int
Au35	0.16				19.38		1.94		Unbarred, int
Au36	0.22				20.88		3.04		Unbarred, int
Au37	0.13				25.38		2.81		Unbarred
Au38	0.40	3.45	5.88	3.40	19.12	18.12	5.05	3.69	Bar
Au39	0.52	5.22	6.52	4.20	21.12	13.04	2.68	1.87	Bar
Au40	0.60	7.12	5.07	5.47	21.88	11.46	3.46	1.74	Bar, int

obtaining the bar length, such as a definition based on the constancy of the phase of the $m = 2$ Fourier mode. We found this latter method to be more prone to noisy bar length estimates, hence why we use the former method here (see also fig. B1 of Fragkoudi et al. 2021).

Disc size, R_d: We define the size of the disc for the galaxies in our sample as the radius at which the stellar surface density drops below $1 M_\odot/pc^2$.

Time at which the galaxy becomes baryon-dominated, $t_{gal,bd}$: We define the time at which the galaxy becomes baryon-dominated, $t_{gal,bd}$, as the time at which the stellar mass begins to contribute at least 80 per cent of the total mass within 5 kpc. In what follows, when referring to the stellar mass of a galaxy, we use the mass within 10 per cent of the virial radius of the galaxy, unless otherwise noted.

The galaxy assembly time, $t_{gal,50}$: is defined as the time at which the galaxy assembles 50 per cent of its stellar mass within a radius of 20 kpc.

$M_\star$: In what follows, we calculate the stellar mass of the simulated galaxy as the mass within 10 per cent of the virial radius, unless otherwise stated.

3 BAR PROPERTIES AND EVOLUTION

We start by exploring some statistical and global properties of bars in our sample (Section 3.1), such as the fraction of bars across stellar mass and redshift, the formation time of bars and their longevity. We then look into one of the most important bar properties, the bar length, its relation to the size of the disc, and how these evolve in time (Section 3.2).

3.1 Global properties of barred galaxies

Bar Formation Time: In Fig. 3, we show the $m = 2$ Fourier mode for the barred galaxies in our sample, as a function of time,
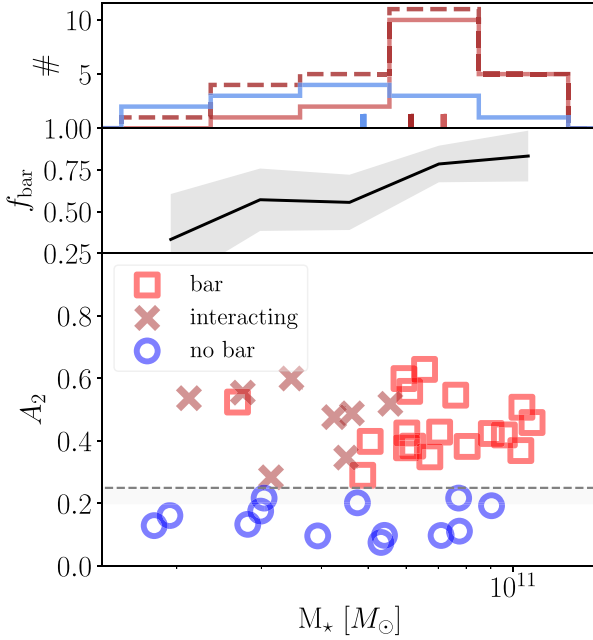
Figure 2. *Top*: Distribution of barred (red), unbarred (blue) and barred + interacting (dashed brown) galaxies in our sample in stellar mass. *Middle*: Fraction of barred galaxies as a function of stellar mass. The shaded area is the uncertainty on the fractions assuming binomial statistics, given by $\sigma = \sqrt{f_{\text{bar}}(1 - f_{\text{bar}})/N}$, where N is the number of galaxies. *Bottom*: Bar strength versus stellar mass for the 40 galaxies in the Auriga suite of simulations. The horizontal dashed line indicates a bar strength of $A_2 = 0.25$, above which we consider the galaxies to be barred. Squares indicate barred galaxies, blue circles indicate unbarred galaxies, and crosses indicate barred galaxies which are undergoing an interaction at $z \sim 0$ (see the text for more details).

colour-coded according to their bar formation time. We see that bars have a wide range of formation times (see also Table 1), with the oldest bar in our sample forming at a lookback time of $t_{\text{lb}} = 10.4$ Gyr and the youngest bar forming at $t_{\text{lb}} = 0.3$ Gyr. It is worth emphasizing that, from $z \sim 1 - 2$, bars in Auriga are long-lived structures, i.e. they do not dissolve and are not recurring. This is evident in Fig. 3 where we see that once a bar forms, i.e. once the bar strength is above $A_2 > 0.25$, it remains above 0.25 and does not go through cyclical periods of destruction and reformation. The single exception to this rule is Au36, whose bar is severely weakened by an interaction with another galaxy, resulting in it being defined as unbarred by $z = 0$ (see Fig. A1; we will explore this system in more detail elsewhere).

Bar fraction: In Fig. 4, we explore the fraction of bars as a function of redshift (and lookback time) in our sample, comparing this to observations from Eskridge et al. (2000), Sheth et al. (2008), and Le Conte et al. (2024). We find that 60 per cent of the galaxies in our sample at $z = 0$ are barred,[3] with the fraction of bars decreasing for higher redshifts and reaching about ~ 20 per cent at $z \sim 3$, in agreement with the aforementioned observations. Beyond

---

[3]This is slightly lower than the fraction found in Fragkoudi et al. (2020), where we only included the 30 high mass Auriga haloes, while here we use $A_2 > 0.25$ to identify bars, as opposed to 0.2 which was employed in our previous study.

$z \sim 1$ there appears to be a slight increase in the bar fraction in our simulations (although not that this is within the uncertainties), indicating that some structures identified as bars at high redshifts might be transient.

The right panel of Fig. 4 shows the bar fraction as a function of lookback time in two stellar mass bins, with masses greater than, and smaller than $M_\star = 5 \times 10^{10} M_\odot$. The right y-axis and grey line indicate the fraction of galaxies in the low mass bin. We find that the bar fraction is higher in the high mass bin at all lookback times at which these galaxies exist in our sample. This emphasizes that at all times, bars are more common in massive galaxies. These findings seem to be compatible with the mass downsizing hypothesis, i.e. that more massive galaxies form bars first (see for example Sheth et al. 2008), but as we show below, this does not necessarily imply a straightforward correlation between the stellar mass of the galaxy and bar formation time.

Mass Build-Up and Bar Formation Time: In the top panel of Fig. 5, we show the bar strength at $z = 0$ as a function of the bar formation time. We find a weak correlation between the bar strength at $z = 0$ and the age (or formation time) of the bar, indicating that older bars tend to be slightly stronger. In the second panel of the figure we show the bar formation time as a function of the time at which the galaxy becomes baryon dominated (see Section 2.2 for details). We see that there is a correlation between these quantities, suggesting that galaxies form a bar when the galaxy passes a threshold of baryon dominance (and see also Section 4.1).

In the bottom panel of Fig. 5, we show the bar formation time as a function of the formation time of the galaxy (which we define as the time at which the galaxy assembles 50 per cent of its stellar mass). We find a strong correlation between the two parameters, indicating that younger bars tend to form in galaxies that assembled their mass later. We note that the yellow point which is an outlier in this relation (Au25) has an underestimated bar age due to the method we use for obtaining the bar formation time. As discussed in Section 2.2, the bar age is taken as the last time A_2 becomes larger than 0.25. This galaxy has a bar strength that oscillates around the cut-off value of 0.25, starting at around $t_{\text{lb}} \sim 3.25$ Gyr. The last time it crosses above 0.25 is at $t_{\text{lb}} = 0.34$ Gyr – making this the bar age according to our definition. However, there is a clearly formed–albeit weak–bar at earlier times already at $t_{\text{lb}} \sim 3.25$ Gyr. The dashed grey line indicates a linear fit to the sample with a slope of 1.6 and intercept of –4.7 Gyr.

In Fig. 6, we explore whether the time of bar formation is correlated to the stellar mass of the galaxy at $z = 0$, as one might naively expect in a mass downsizing scenario. In the middle panel, we show the formation time of the bar as a function of the stellar mass of the galaxy at $z = 0$, in which we do not find a correlation. Nor do we find a correlation between bar formation time and the stellar mass of the galaxy at the time of bar formation, as is shown in the right panel of Fig. 6 – indeed we find a weak anticorrelation between these quantities. This can be understood since bars that form at higher redshifts will form in galaxies that have not yet fully assembled their stellar mass. On the other hand, we see that the formation time of the bar correlates (albeit weakly) with how much the stellar component dominates over the dark matter component within 5 kpc at $z = 0$, as can be seen in the left panel of Fig. 6. This indicates that at $z = 0$, we can relate how old a galaxy's bar is, with how baryon-dominated that galaxy is. It is worth noting the scatter in this relation, which increases at older ages, likely due to effects related to mergers which, as we will see below, can also act as triggers of bar formation.
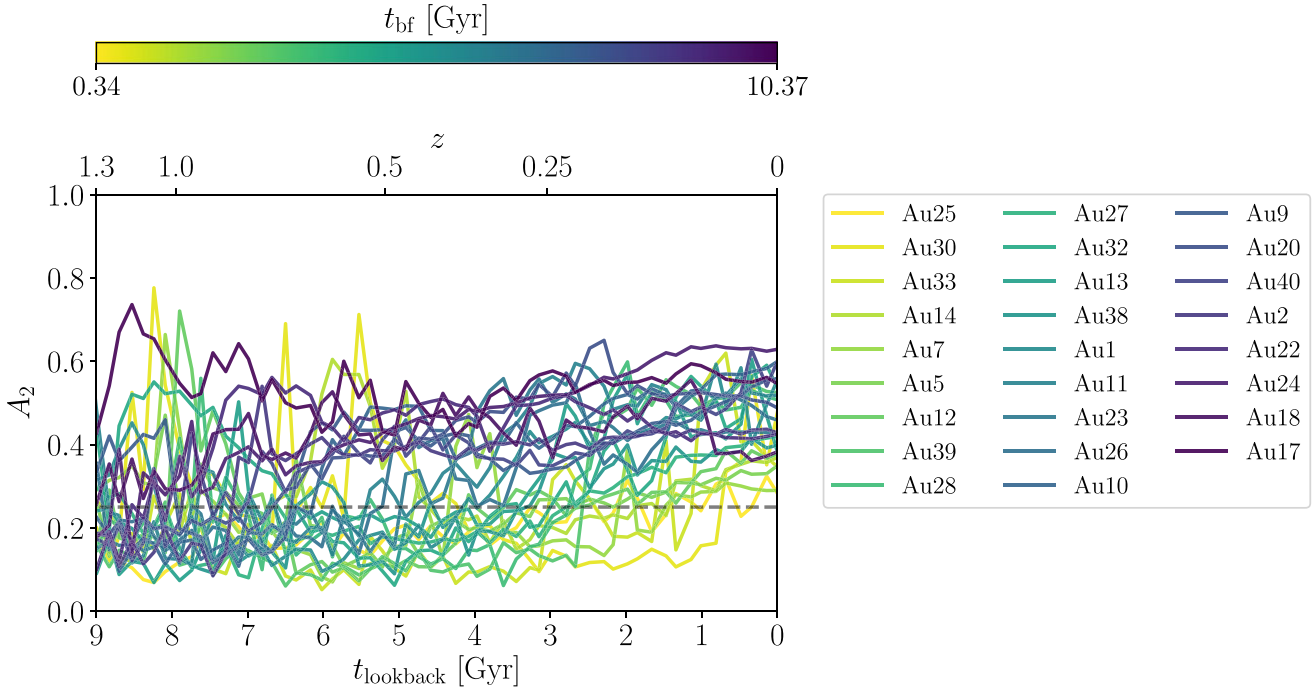
Figure 3. The $m = 2$ Fourier mode of the surface density as a function of lookback time for galaxies which are barred at $z = 0$. The lines are sorted by the formation time of the bar (dark purple: bar forms at larger lookback time, light yellow: bar forms close to $z = 0$). The galaxies that end up barred at $z = 0$ develop their bars at various times in the simulation, some forming early on and staying barred, while others have bars that develop only at late times.
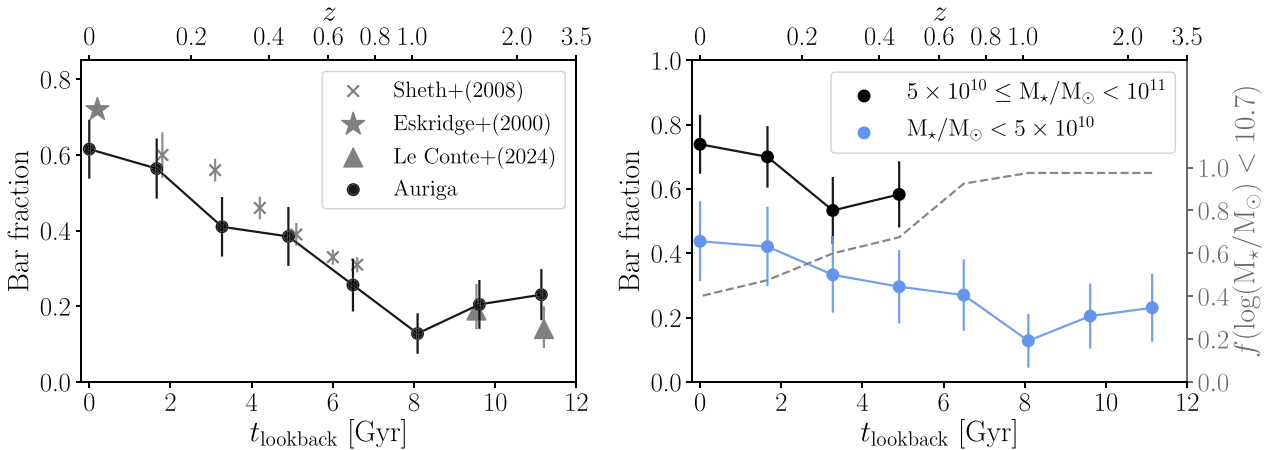
Figure 4. Statistical properties of the entire sample of 40 Auriga galaxies. *Left*: Bar fraction as a function of redshift (top axis) and lookback time (bottom axis) for the suite of Auriga simulations, compared to observations from Eskridge et al. (2000), Sheth et al. (2008), and Le Conte et al. (2024). *Right*: Bar fraction as a function of redshift for galaxies in two stellar masses bins, as indicated in the legend. The right axis and grey line indicate the fraction of galaxies in the low-mass bin. We note that in these plots, time is plotted in the opposite direction from the other plots in the paper, in order to match the convention used in observational studies. We find a decreasing bar fraction with redshift in the Auriga simulations, and that more massive galaxies host more bars at all the times we are able to explore.

3.2 Evolution of bar properties

In this section, we explore the evolution of bar properties in Auriga as a function of time, focusing in particular on the length of bars and the ratio of bar length to disc size.

In Fig. 7, we show the evolution of bar length as a function of time. In particular, we group together bars according to their formation time, i.e. we select bars that form between lookback times of $t_{lb} = 0$–2.7 Gyr ago (dark purple), $t_{lb} = 2.8$–4.9 Gyr (dark blue),

$t_{lb} = 5$–7.1 Gyr (dark green), and $t_{lb} = 7.2$–11 Gyr (light green), as indicated by the legend. These bins are chosen such that they split the sample into 4 groups with approximately the same number of galaxies. We find that bars that form at low redshifts, tend to form shorter bars which subsequently grow longer over time.

On the other hand, bars that form at higher redshifts (e.g. around $z \sim 1$ – see the green line) tend to already be quite long when they form, and their length does not evolve much over the galaxy's
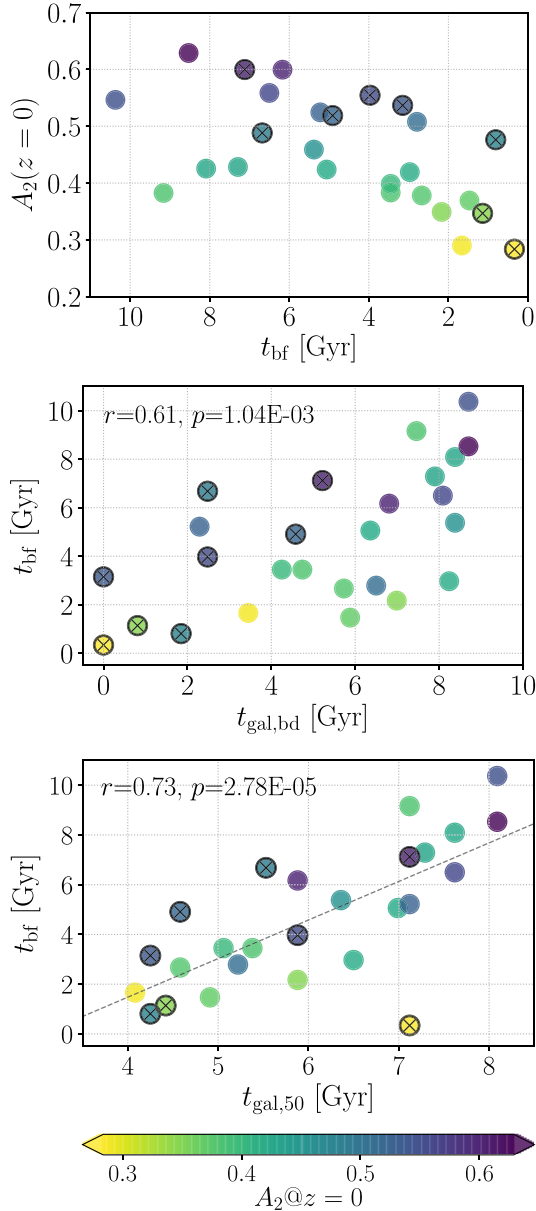
Figure 5. *Top*: Bar strength at $z = 0$ versus the age of the bar. The colour-coding gives the bar strength (used in subsequent plots). The points outlined in black denote the 'interacting' sample (see the text and Table 1). *Middle*: Bar formation time as a function of the time at which the galaxy becomes baryon-dominated. We indicate the Pearson coefficient, r, and the p-value for the entire sample of galaxies in the top left. *Bottom*: Bar formation time as a function of the time at which the galaxy assembles 50 per cent of its stellar mass. The dashed line indicates the linear regression fit for the non-interacting galaxies (see the text).

lifetime. We hypothesize that this is due to the fact that galaxies that form bars at high-z are triggered by a merger, and therefore form long and 'saturated', i.e. they are not able to grow by exchanging more angular momentum. Indications of this can be seen in the inset of Fig. 7, where we show the time of one of the three most massive mergers in the galaxy, versus the time of bar formation. We see that the galaxies that form bars at high redshift all do so around the time of one of their most massive mergers. The growth of bars is mediated through the exchange of angular momentum between the

inner disc and the outer disc and halo, with the disc acting as an 'emitter' and the halo acting as a 'sink' of angular momentum (see e.g. Athanassoula 2003). We speculate that if a bar forms through a merger/interaction, the torques induced in this process might reduce the amount of angular momentum able to be exchanged. This could be because of the torques induced in the disc which can trigger the bar to form in the first place (see e.g. Łokas 2018; Merrow et al. 2024) or it could be due to the injection of angular momentum in the halo via the interaction/merger, which therefore means the halo is able to absorb less angular momentum. These processes could therefore lead to the angular momentum exchange being 'saturated', which can impede the further growth of the bars. While there are hints of this in the simulations (e.g. the fact that the bars forming at high redshifts all form around the time of a significant merger, and that they do not grow longer in time), this hypothesis would need to be investigated in more detail, which we defer to future work.

We quantify these trends further in Fig. 8, where we plot the bar length of galaxies as a function of the formation time of the bar, in the left panel at the time of bar formation, and in the middle panel at $z = 0$. In the right panel we show the relative change in the bar length from the time of bar formation until $z = 0$ for each galaxy. This quantifies the bar growth for the various galaxies, reinforcing the fact that the oldest bars undergo less growth – as they already form long – while the bars that undergo the most growth are those of intermediate ages. The youngest bars also grow in time, but as they have less time to evolve than the intermediate age bars, their relative growth is limited.

Given that galaxies tend to have smaller discs at higher redshifts (e.g. van der Wel et al. 2014; Ormerod et al. 2024), it might be somewhat surprising that bars that form early on in the Universe in our simulations have longer bars. This would imply that the ratio of bar length-to-disc size changes as a function of redshift. We explore the ratio of bar length to disc size in Fig. 9; we focus here on the non-interacting barred galaxies, since interacting galaxies have disturbed discs and as such the concept of the disc size becomes ambiguous. In the left panel of the figure we show the ratio of bar length-to-disc size *at the time of bar formation* for each of the galaxies, as a function of bar formation time. We find a trend in which this ratio is higher for galaxies whose bars form at higher redshifts. We therefore see that when bars form at high redshifts they extend over a larger range of the disc. In the middle panel we show this ratio at $z = 0$, and in the right panel we show the change in the ratio from the time of bar formation until $z = 0$. In the middle panel it is clear that the bar length-to-disc size relation flattens out by $z = 0$. By examining the middle and right panels of the figure, we see that the ratio decreases for the older bars, due to the fact that the disc size increases for these galaxies, while the bar length doesn't increase significantly (as shown in Figs 7 and 8). On the other hand, for the younger bars the ratio increases at $z = 0$, which is due to the increase in the bar length for intermediate and young bars over time. Therefore, when observing bars at higher redshift, we might expect to find a higher bar-to-disc size ratio than in the local Universe.

4 DRIVERS OF BAR FORMATION

In this section we explore the various factors that are thought to be important for the formation of bars – namely the baryon-dominance (4.1), accreted bulge component (4.2), gas fraction (4.3), and the Toomre Q parameter (4.4) – examining the role these play in bar formation within the cosmological context.
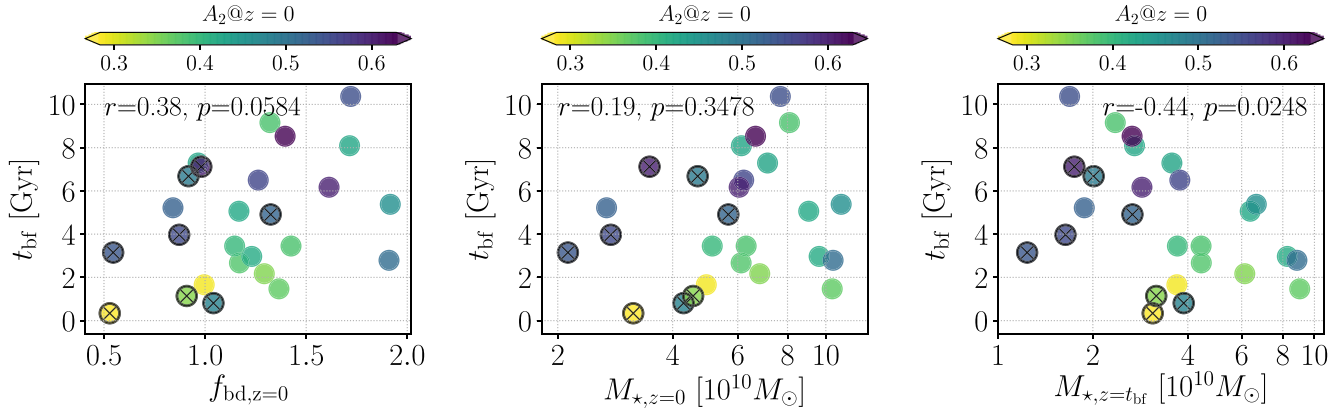
Figure 6. Bar formation time as a function of various parameters. Black circles denote the interacting galaxies and the Pearson coefficient, r, and p-value are indicated at the top of each panel: *Left:* Bar formation time as a function of the stellar-to-dark matter ratio inside 5 kpc at $z = 0$. *Middle:* Bar formation time as a function of the stellar mass of the galaxy at $z = 0$. *Right:* Bar formation time as a function of the stellar mass of the galaxy at the time of bar formation. There is a mild correlation between the bar formation time and the stellar-to-dark matter ratio at $z = 0$, while there is no significant correlation between bar formation time and stellar mass at $z = 0$ (i.e. no obvious signs of mass downsizing within this mass range). There is a trend of decreasing stellar mass for earlier bar formation time (right panel), as expected, since galaxies at higher redshifts have lower stellar masses.
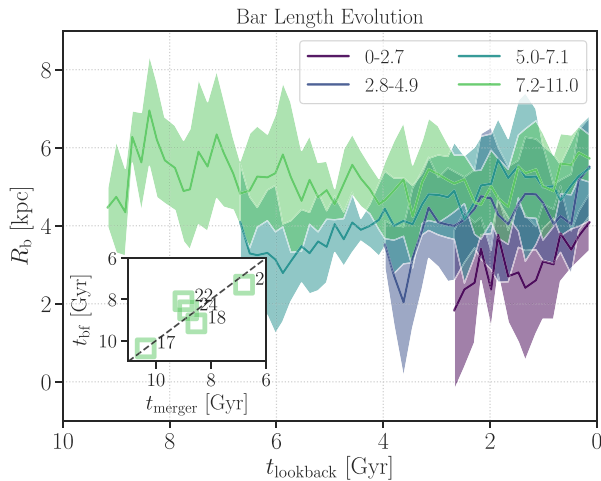
Figure 7. Bar length as a function of time for galaxies that form bars between four different time-frames, as indicated by the figure inset. The solid lines show the average values of the bar length and the shaded region shows the 1σ dispersion. We see that bars that form at high redshifts tend to already form long, while bars forming at low redshifts form short and grow longer with time. The inset compares the time of significant merging events to the time of bar formation for the oldest bars, with the dashed line indicating the 1-to-1 line. The oldest bars in our sample seem to form around the time of a significant merger event.

4.1 Baryon dominance

It is well established that the ratio of the stellar disc to the dark matter halo mass within a spiral galaxy is a determining factor in how unstable the galaxy will be to the formation of a bar (e.g. Ostriker & Peebles 1973; Combes et al. 1990; Athanassoula 2002; Fujii et al. 2018). Here, we explore how the baryon-dominance of a galaxy affects the formation of a bar in the Auriga cosmological simulations.

As discussed in Section 3.1, in the bottom panel of Fig. 5 we compare the bar formation time to the time at which the galaxy has at least 80 per cent of the total mass within 5 kpc dominated by the stellar component (which we define as the time at which the galaxy

becomes baryon-dominated). We find that there is a correlation – albeit with significant scatter – between the time at which the bar forms and the time at which the galaxy becomes baryon-dominated, suggesting that once a disc becomes baryon-dominated it will tend to form a bar.

To further explore the role baryon-dominance plays on bar formation in the cosmological context, in Fig. 10, we show the stellar mass against the halo mass for the galaxies in our sample, which are labelled according to whether they are barred, unbarred, or have a bar but are also interacting at $z \sim 0$. We also plot the abundance matching relation from Moster et al. (2013) for comparison. We find that barred galaxies tend to be displaced from the commonly used abundance matching relation, as compared to unbarred galaxies, which lie closer to the relation. We quantify this offset from the abundance matching relation in the top right panel of Fig. 10: we show the vertical displacement of the galaxy from the abundance matching relation (i.e. the over- or under-abundances in stellar mass as compared to the abundance matching relation, for a given halo mass), normalized by the 1σ scatter of the abundance matching relation of Moster et al. (2013). The barred galaxy sample is shown in red, the unbarred sample in blue, and the barred sample including the interacting galaxies with the dashed brown line. We see that barred galaxies tend to be more than 2σ offset from the abundance matching relation, compared to unbarred galaxies which lie closer to the abundance matching relation. The vertical arrows indicate the median value for each population. It is worth noting that this 'offset' from the abundance matching relation correlates to the baryon-dominance f_{bd} of the galaxy, as can be seen in Fig. B1. The bottom right panel of Fig. 10 shows the $V_\star/V_{tot}$ of the barred and unbarred galaxies in our sample, and in black for the Milky Way (as determined by Bovy & Rix 2013). We see that barred galaxies have higher $V_\star/V_{tot}$ than unbarred galaxies at all radii. However, this is not as high as that for the Milky Way, suggesting that Milky Way-like galaxies in cosmological simulations might still be less baryon-dominated than massive spiral galaxies in the local Universe. This fact, i.e. that cosmological simulations are not as baryon-dominated as suggested by dynamical models of massive spiral galaxies in the local Universe (e.g. Weiner, Sellwood & Williams 2001; Kranz, Slyz & Rix 2003; Fragkoudi, Athanassoula & Bosma 2017a), is commonly found in
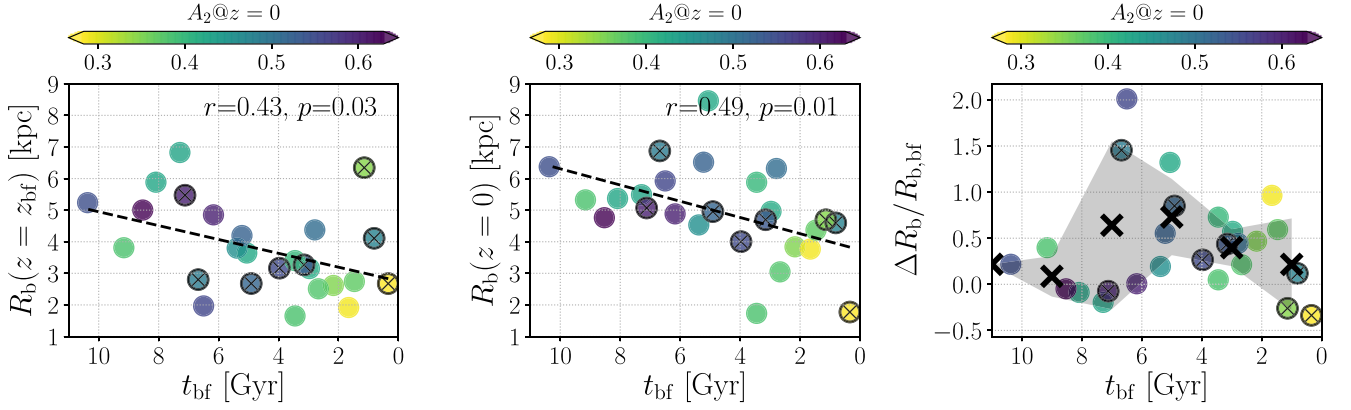
Figure 8. Bar length as a function of the formation time of the bar for the entire barred sample (interacting galaxies have black circles). *Left*: The bar length at the time of bar formation, as a function of bar formation time. *Middle*: The bar length at $z = 0$ for these same galaxies, as a function of the bar formation time. *Right*: The relative change in the bar length as a function of bar formation time. The crosses indicate the average value for a given age bin, and the shaded region shows the 1σ spread. Bars that form at high redshifts do not change their lengths much because they form long already, while the youngest bars have had limited amount of time to grow their bar length.
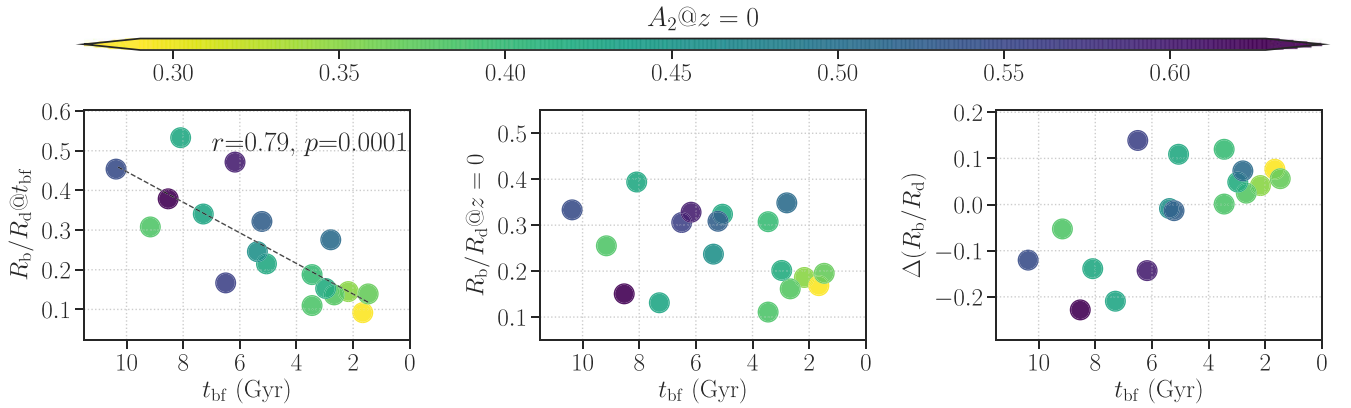
Figure 9. The bar length-to-disc size ratio as a function of the formation time of the bar for the non-interacting galaxies. *Left*: The ratio at the time of bar formation. *Middle*: The ratio at $z = 0$. *Right*: The change in the ratio from bar formation time to $z = 0$. We see that the ratio of bar length-to-disc size is larger at the time of bar formation for early forming bars, and decreases at $z = 0$ due to the increasing disc size.

the literature (Lovell et al. 2018; Posti, Fraternali & Marasco 2019; Fragkoudi et al. 2021; Posti & Fall 2021).

In Fig. 11, we explore the ratio of stellar-to-dark matter within 5 kpc (f_{bd}) as a function of time; we find that, already at earlier lookback times, the barred galaxies are more baryon dominated than the unbarred sample which remains dark matter dominated even at low redshifts. This trend also holds if we explore the baryon dominance within the half-mass radii of the galaxies (r_{50}), as is shown in Fig. B3, with the differences between the two populations being even more pronounced (due to the fact that the half-mass radii of barred galaxies are smaller than for unbarred galaxies in our sample).

In Fig. 12, we show the growth of the stellar mass of the barred (red) and unbarred (blue) galaxies as a function of time. As discussed in Section 2.2, we calculate the stellar mass within 10 per cent of the virial radius of the galaxy. We find that barred galaxies assemble their stellar mass more rapidly than unbarred galaxies (see also Rosas-Guevara et al. 2020). We quantify this by exploring when the samples assemble 50 per cent of their stellar mass, and find that barred galaxies assemble their stellar mass on average ∼1 Gyr earlier than unbarred galaxies. Barred galaxies therefore tend to grow their

stellar component more rapidly than unbarred galaxies, forming an early massive stellar disc, which is conducive to bar formation.

4.2 The *ex situ* bulge

We now explore how the fraction of *ex situ* (accreted) stars in the central regions of galaxies affects the formation of bars. The fraction of accreted stars in the inner regions can be thought of as a proxy for a merger-built hot (classical) component, since these accreted stars will be brought in via mergers. For example, Gargiulo et al. (2022) showed that simulated galaxies whose bulge has a high Sérsic index will also tend to have a larger fraction of *ex situ*. As hot spheroids (either stellar or dark matter) have been shown to delay the formation of bars (e.g. Ostriker & Peebles 1973; Athanassoula 2002), one might expect such an *ex situ* component to have an impact on bar formation in cosmological simulations. We use the fraction of *ex situ* stars rather than a kinematic characterization of the bulge because commonly-employed kinematic estimates (such as the circularity parameter Abadi et al. 2003) are affected by the presence of a bar (which induces large non-circular motions in the orbits of stars in the central region). This makes it challenging to separate the contribution of the spheroid
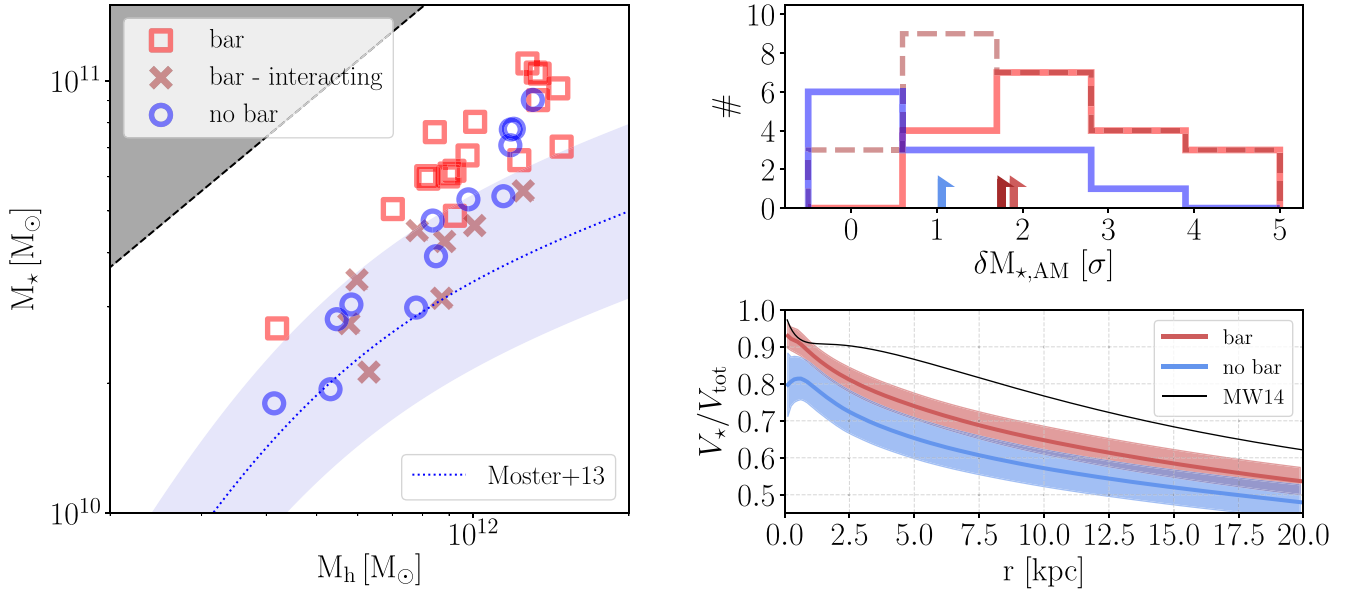
Figure 10. *Left*: The loci of galaxies in our sample in the stellar mass–halo mass plane at $z = 0$. We indicate whether the galaxy is unbarred (blue circle), barred (red square) or barred and undergoing an interaction at $z = 0$ (cross). The abundance matching relation from Moster, Naab & White (2013) is indicated with the blue line and shaded region. *Top Right*: The distance of galaxies from the abundance matching relation for barred (red), unbarred (blue), and barred + interacting (dashed brown) galaxies. *Bottom right*: The baryon-dominance as a function of radius of the barred (without interacting galaxies; red) and unbarred (blue) galaxies in our sample, as indicated by $V_\star/V_{tot}$. We compare these to the Milky Way model from Bovy & Rix (2013) (black). While barred galaxies are on average more baryon-dominated than unbarred galaxies in Auriga, both are less baryon-dominated than the MW14 model for the Milky Way.
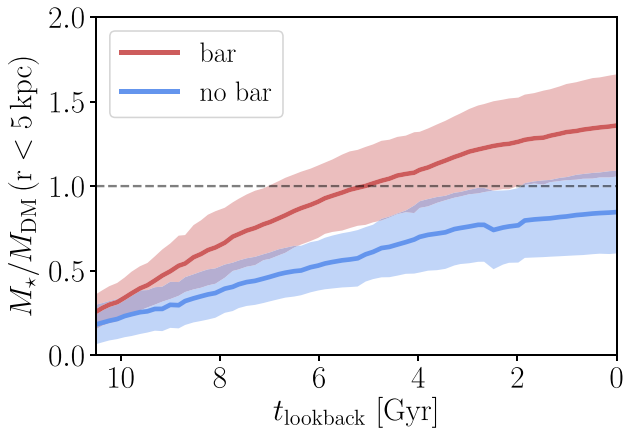
Figure 11. The average (solid lines) and standard deviation (shaded regions) of the ratio of stellar-to-dark matter mass within 5 kpc as a function of time for the barred galaxies (excluding the interacting galaxies), in red, and for the unbarred galaxies, in blue. On average, for barred galaxies, the stellar mass dominates over the dark matter mass within the central 5 kpc by $z \sim 0$, which is in contrast to unbarred galaxies which tend to be more dark matter dominated over all cosmic times.

from the bar. In what follows we consider the accreted fraction within the inner 5 kpc, but we note that our results are qualitatively similar when considering different radii.

We start by comparing in Fig. 13 the fraction of accreted stars in the bulge, for the barred and unbarred galaxies in our sample (see also Fragkoudi et al. 2020). We compare unbarred galaxies to barred galaxies (excluding interacting galaxies at $z = 0$) and find that unbarred galaxies have ×2 higher fraction of accreted stars; this supports the previous theoretical results that have found that massive
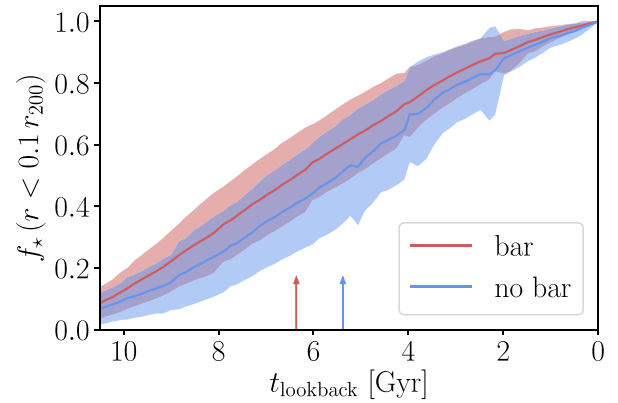
Figure 12. The build-up of stellar mass in barred (without interacting) and unbarred galaxies as a function of time. The solid lines show the average values for the samples and the shaded regions the 1σ dispersion. Barred galaxies tend to build up their stellar mass more rapidly than unbarred galaxies, with the time at which they build up 50 per cent of their stellar mass roughly 1 Gyr earlier than for unbarred galaxies (indicated by the red and blue arrows, respectively).

classical bulges can impede bar formation. The difference in the accreted bulge fraction between barred and unbarred galaxies becomes somewhat less prominent if we include the interacting galaxies in the barred sample (see middle column of Fig. 13), however the unbarred galaxies still have ~ 50 per cent higher accreted fraction in the bulge as compared to the total barred sample. Similar results were found previously in Fragkoudi et al. (2020) for the Auriga galaxies and in Gargiulo et al. (2022) for the ILLUSTRISTNG50 simulations, who found that galaxies with a low fraction of *ex situ* stars in their bulge are more likely to host a long-lived bar.
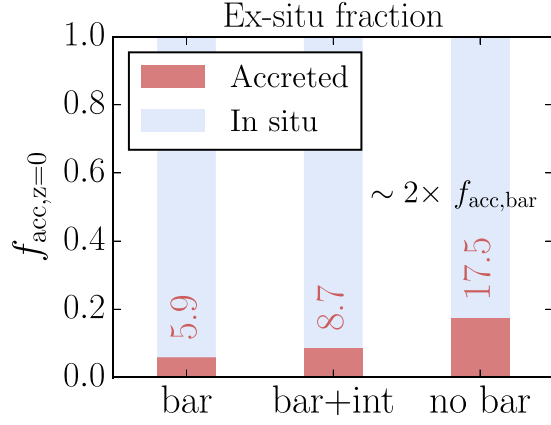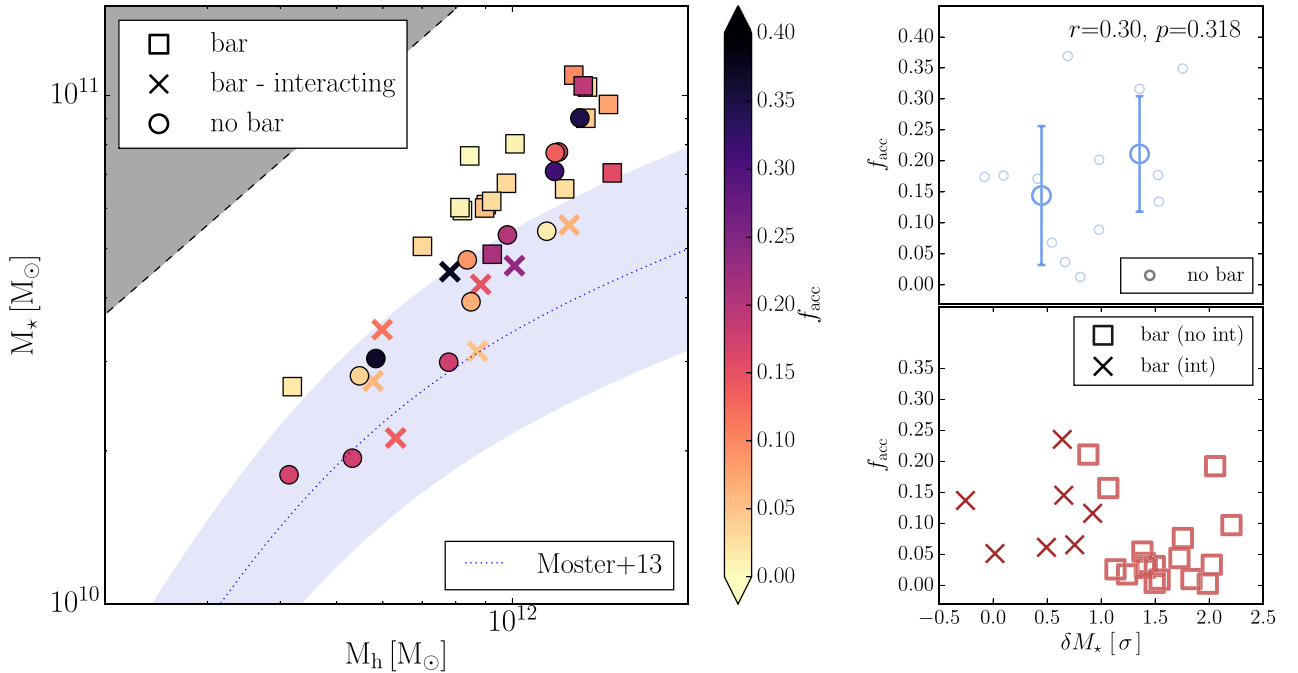
Figure 13. Average fraction of accreted stars in the 'bulge', at $z = 0$, for the barred (without and with interacting galaxies, left and middle) and unbarred (right) galaxies in our sample. Unbarred galaxies have on average $\sim 2\times$ more *ex situ* stars in their bulge than the barred sample (without interacting galaxies) and 60 per cent more *ex situ* stars in the bulge than the total barred sample.

We further investigate whether the accreted fraction can prevent galaxies from forming bars by exploring how this relates to the baryon-dominance of galaxies. As discussed in the previous section, galaxies that are more baryon-dominated are more likely to form a bar. However, there are some galaxies in our sample which *are* baryon-dominated (and offset from abundance matching relation – see Fig. 10), which have not formed a bar by $z = 0$, indicating that something may be preventing them from forming a bar. In Fig. 14, we explore how the offset from the abundance matching relation

depends on the accreted fraction of stars for unbarred galaxies. In the left panel, we plot the $M_\star - M_h$, colour-coded by the faction of accreted stars. We see that galaxies that are baryon-dominated, i.e. are offset from the abundance matching relation, which do not host a bar, also tend to have a higher fraction of accreted stars. This is shown explicitly in the top right panel of Fig. 14, where we plot the fraction of accreted stars versus the offset from the abundance matching relation for the unbarred galaxies in our sample. While there is not a strong correlation between the two parameters, we find that galaxies that are more offset from the abundance matching relation tend to have a higher fraction of accreted stars. This seems to suggest that having a higher fraction of accreted stars could suppress the formation of the bar, even when the galaxy is baryon-dominated. On the other hand, there is no obvious trend for the barred galaxies with accreted fraction (see bottom right panel of Fig. 14), and as already mentioned, these galaxies tend to have lower accreted fractions.
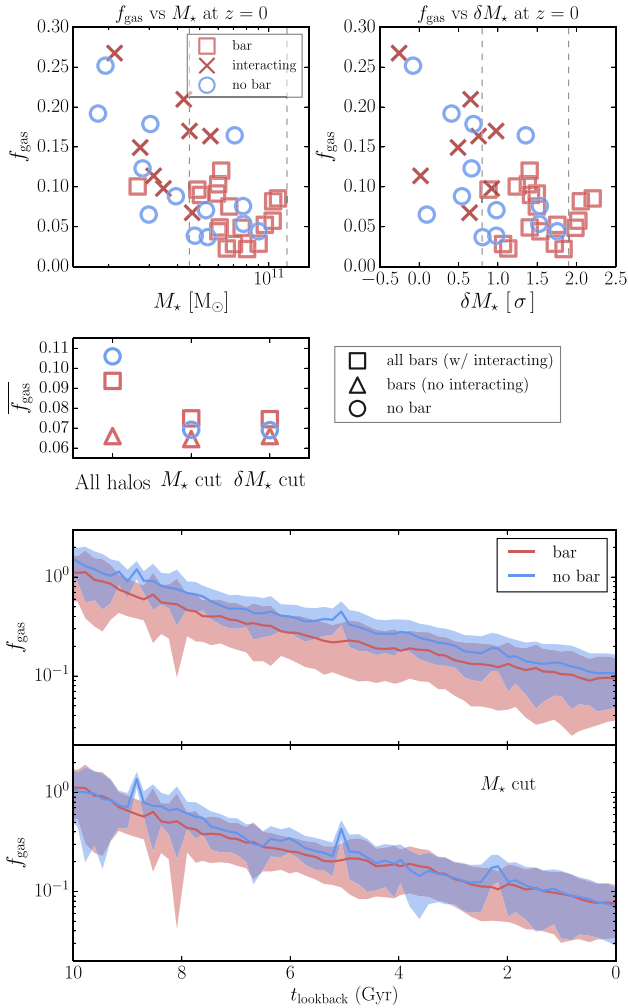
4.3 Gas fraction

In Fig. 15, we show the fraction of gas in barred and unbarred galaxies at $z = 0$ within a radius of $r = 5$ kpc, in order to explore the effect it has on bar formation in cosmological simulations. We focus on the gas fraction within the inner regions of the disc where the bar is, as that is where it will have the largest effect on the bar dynamics. In the top left column, we show the gas fraction as a function of stellar mass. In the top right column, we show the gas fraction as a function of the offset from the abundance matching relation (which as discussed previously, correlates with the baryon-dominance). We see that there is an overall decrease in the gas fraction for higher stellar mass galaxies, while a similar decrease in gas fraction can be seen as a function of baryon-dominance, with both barred and unbarred galaxies occupying similar regions in these planes. Interestingly, in

Figure 14. The relation between the $M_\star - M_h$ plane and the fraction of *ex situ* stars in the central 4 kpc. *Left*: The $M_\star - M_h$ plane colour-coded by the accreted fraction of stars in the bulge. *Right*: The fraction of accreted stars in the bulge as a function of the offset from the abundance matching relation for the unbarred galaxies (top) and the barred galaxies (bottom). We see that galaxies that are more offset from the abundance matching relation tend to have higher *ex situ* fractions, indicating that the *ex situ* bulge contributes to suppressing bar formation in baryon-dominated systems.

Figure 15. The effect of gas fraction on bar formation: *First row*: At $z = 0$, the gas fraction for each halo as a function of stellar mass (left) and as a function of the baryon-dominance of the galaxy (right). The vertical dashed lines indicate the range in which galaxies are considered for the averages shown in the panel below. *Second row*: The average gas fraction for various samples: All galaxies, galaxies with the $M_\star$ and $\delta M_\star$ cuts shown above, separating into all the bars, bars excluding interacting galaxies and unbarred galaxies. *Third row*: The gas fraction for all barred and unbarred galaxies in our sample across time. *Fourth row*: As above, but for galaxies within the mass range shown in the top left panel. If we consider galaxies in a given mass bin, the gas fractions are the same for barred and unbarred galaxies.

the top panel, we see that the barred galaxies that have lower masses (and high gas fractions) are also the ones that appear to have had a recent interaction.

In the middle left panel of the figure, we show the average gas fraction in the barred sample, with and without interacting galaxies (square and triangle points, respectively) and unbarred galaxies (circle), in the leftmost point (labelled 'All haloes'). We find that when considering all galaxies in our sample, unbarred galaxies tend to have higher gas fractions (by about ~ 13 per cent) than barred galaxies. This is accentuated (to ~ 60 per cent higher gas fraction) when comparing unbarred galaxies to barred galaxies which are not interacting. This might lead one to conclude that the gas fraction is higher for unbarred galaxies; however, as there is a dependence

of bar fraction on stellar mass – see e.g. in Fig. 2 – we repeat this measurement by factoring out the mass dependence. That is to say, since there is an anticorrelation between gas fraction and stellar mass (i.e. low mass galaxies tend to have higher gas fractions), it is unclear whether the average higher gas fractions of unbarred galaxies could be due simply to the fact that low mass galaxies in our sample tend to be unbarred. To factor out the stellar mass dependence, we apply a mass cut as indicated by the vertical dashed lines in the top left panel, and recalculate the average gas fraction for our three samples in that mass range; this is shown in the middle left panel (labelled '$M_\star$ cut'). We also explore the average gas fraction for a given baryon-dominance cut (labelled '$\delta M_\star$ cut'), with the restricted range shown with the vertical lines in the top right panel. We find that both when restricting our sample to a smaller range in stellar mass or baryon-dominance, the average gas fractions of barred and unbarred galaxies are very similar, differing by less than 3 per cent.

In the two bottom panels of Fig. 15, we show the gas fraction within 5 kpc for barred and unbarred galaxies as a function of time. In the second to last panel, we see that unbarred galaxies tend to have slightly higher gas fractions across time. However, in the bottom panel we see that, if we restrict the sample to galaxies within the same mass bin (as in the top left panel of Fig. 15), we find similar gas fractions for both barred and unbarred galaxies across all cosmic times.

We therefore conclude that, gas fraction does not seem to be a driving factor of bar formation in and of itself, since if we restrict our samples to a given stellar mass, or indeed a given baryon-dominance, barred galaxies do not tend to be more gas rich. Rather the difference in average gas fractions in the barred and unbarred sample over all stellar masses, seems to be a consequence of the dependence of gas fraction on stellar mass, which sets how baryon-dominated the galaxies are.
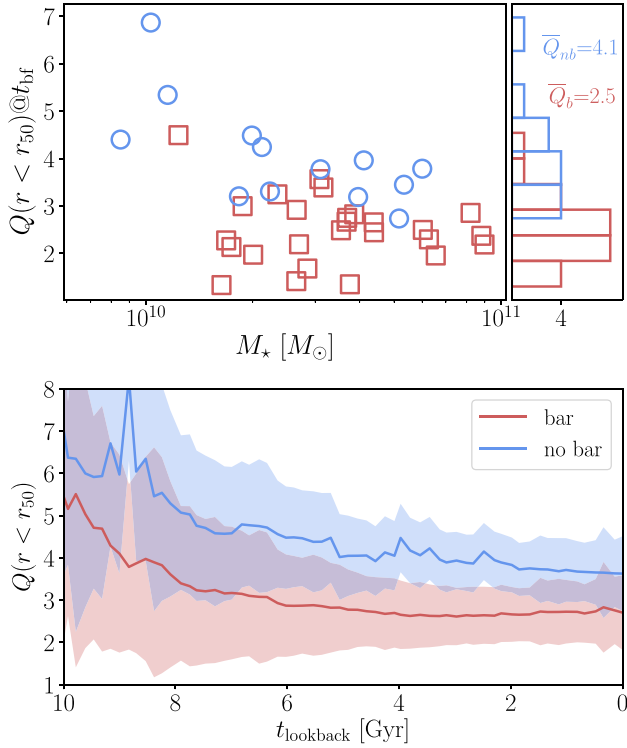
4.4 The Toomre Q parameter

A parameter which is known to play an important role in the formation of bars is the in-plane radial velocity dispersion of the stellar component (e.g. Combes & Sanders 1981; Athanassoula & Sellwood 1986), which affects how cold the disc is, and therefore its stability. This has often been explored in the literature by examining the dependence of bar properties on the Toomre Q parameter (Toomre 1964),

$$Q = \frac{\sigma_r \kappa}{3.36 G \Sigma_\star}, \tag{4}$$

where σ_r denotes the radial velocity dispersion of the stellar disc, κ the epicyclic frequency, G Newton's gravitational constant, and $\Sigma_\star$ is the surface density of the stellar disc.

In the top panel of Fig. 16, we show the average Toomre Q parameter within the stellar half mass radius of the barred and unbarred galaxies in our sample at the time of bar formation, as a function of stellar mass (for the unbarred galaxies, we calculate this parameter at 4.6 Gyr, which corresponds to the average time of bar formation for the galaxies in our sample). We see that the unbarred galaxies have a higher Toomre Q parameter than the barred galaxies. This occurs for all stellar masses.

In the bottom panel of Fig. 16, we plot the average and 1σ dispersion for Q within the half-mass radius for barred (red) and unbarred (blue) galaxies, as a function of time. We see that unbarred galaxies tend to have higher Q across all times, although the

Figure 16. The Toomre Q parameter for the galaxies in our sample. *Top*: Toomre Q inside stellar r_{50} at the time of bar formation, for barred (red squares) and unbarred (blue circles) galaxies, as a function of the stellar mass of the galaxy at that time (note that for the unbarred galaxies we take these values at the time corresponding to the average bar formation time – see the text). Unbarred galaxies tend to have higher Toomre Q than barred galaxies at the time of bar formation for all stellar masses. *Bottom*: The average Toomre Q inside r_{50} for barred (red) and unbarred (blue) galaxies in our sample as a function of time.

difference between the two samples decreases slightly at lower redshifts.

We therefore find that the in-plane radial velocity dispersion – and therefore the stability of the disc – does play a role in determining whether a galaxy will be barred or unbarred in cosmological simulations. As the galaxy's formation history will determine the radial velocity dispersion within the galaxy (both in the innermost regions and in the disc), the relation between the galaxy's formation history and Toomre Q is worth exploring in future work.

5 DISCUSSION

In what follows we discuss the implications of our results in terms of the baryon-dominance of galaxies on the TF relation (Section 5.1) and what our findings about the evolution of bars imply about bars at high redshift (Section 5.2).

5.1 Implications for the TF relation

The TF (Tully & Fisher 1977) is an empirical relation between the rotation velocity of galaxies – often the radius at which the rotation curve flattens out – versus their luminosity. This relation has low intrinsic scatter, making it a powerful tool for determining distances to galaxies, while it has also proved useful for testing galaxy formation models in Lambda cold dark matter (Mo, Mao &

White 1998) and theories of modified gravity, such as Modified Newtonian Dynamics, or MOND (see e.g. Milgrom 1983; McGaugh 2012). In Fig. 17, we explore the consequences of our findings in Section 4.1 – i.e. the fact that barred galaxies tend to be more baryon-dominated than unbarred galaxies – on the stellar TF relation (STFR; in Appendix 6 we show results for the Baryonic TF relation). We obtain the circular velocity at $z = 0$ of the galaxies in our sample at 30 kpc – which corresponds roughly to the flat part of the rotation curve for the galaxies we are exploring, i.e. V_{flat}. We then fit the relation $\log M_{\star} = m \log V_{\text{flat}} + y_0$ to our sample of barred galaxies (excluding interacting galaxies) and unbarred galaxies. In the left panel of Fig. 17, we show a least squares fit to this sample (grey dashed curve). The vertical scatter of the relation in our sample is $\sigma_y = 0.05$dex, as indicated with the grey shaded region. In the right panel of the figure, we fit separately the barred (red) and unbarred (blue) samples. For these fits, we fix the slope of the relation to be that obtained for the total sample and we perform bootstrapping to assess the uncertainties in the fits. The 95 per cent percentile uncertainty in the intercept, as obtained from our fits, is shown with the shaded regions. We find an offset in the STFR of the barred galaxies as compared to that of the unbarred galaxies, of the order of $\Delta y_0 = 0.05$ dex. This offset is comparable to the intrinsic scatter of the entire sample, suggesting that, while challenging, it could in principle be observed.

We now turn our attention to what observational studies have found regarding the barred and unbarred TF relation. There have been few of these carried out in the literature, often finding antithetical results. For example, the study of Sakai et al. (2000) found that the TFR of barred galaxies is offset from the unbarred one, suggesting that barred galaxies have maximal discs. The subsequent study of Courteau et al. (2003) explored this in two separate samples, the Shellflow and SCII surveys. Courteau et al. (2003) found a difference in the TFR for barred and unbarred galaxies in the Shellflow survey, while they did not find any offset in the SCII sample. Due to the marginally larger number of galaxies in the latter sample, the authors concluded that there is no difference between the barred and unbarred TFR. We note that these studies did not have resolved H I rotation curves, which would therefore increase the scatter in the relation (e.g. Ponomareva et al. 2017). Therefore, the question of whether the barred TFR is offset from the unbarred one in observational samples still remains, and would be worth exploring with more recent and larger samples.

It is worth emphasizing, that should such a trend be confirmed in the observed barred and unbarred TFR, this would be a strong indication for the existence of dark matter, since such an offset cannot be naturally explained in a modified gravity framework, such as in Modified Newtonian Dynamics (MOND; Milgrom 1983; McGaugh 2012). In a MONDian framework, the V_{flat} would be exactly proportional to the enclosed mass, and as such the relation should not have any intrinsic scatter (see e.g. McGaugh et al. 2000). Finding an offset between barred and unbarred galaxies would be indicative of intrinsic scatter in the relation, which is more naturally explained in a framework with dark matter, i.e. where barred galaxies are more baryon-dominated in the inner regions, with the stellar component of the disc dominating over the dark matter halo.

5.2 Bars at high-z

A number of observational studies have explored the fraction of barred galaxies between redshifts of $z = 0$–1, with most studies finding a declining bar fraction as a function of redshift (Abraham et al. 1999; Sheth et al. 2008; Melvin et al. 2014; Simmons et al. 2014), although some studies find constant bar fractions (specifically
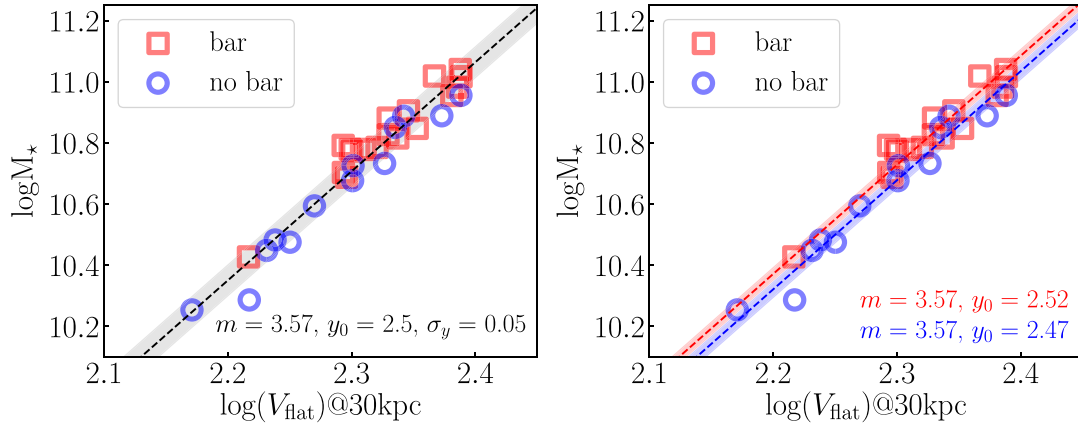
Figure 17. The stellar TF relation at $z = 0$ for galaxies in Auriga barred galaxies (excluding interacting) and unbarred galaxies. *Left*: The grey dot–dashed line shows the relation given by fitting all galaxies together, while the shaded region indicates the intrinsic vertical scatter σ_y. *Right*: The red (blue) dashed line shows the relation when fitting only the barred (unbarred) galaxies. The shaded regions indicate the uncertainties from boostrapping (see the text). We find that the TF relation for barred galaxies is offset from that of the unbarred galaxies.

for strong bars) (Jogee et al. 2004). Studies using data from the *HST* have found that by $z = 1$, the bar fraction drops to ~ 10 per cent (e.g. Simmons et al. 2014). Recent studies using JWST data have been revealing barred galaxies at $z > 1$ (e.g. Guo et al. 2023), and shedding new light on the bar fraction at these redshifts. For example, a recent study by Le Conte et al. (2024) – covering the redshift range $z = 1$–3 with data from the Cosmic Evolution Early Release Science Survey (CEERS; Finkelstein et al. 2023) – found that compared to previous *HST* results, the fraction of bars is higher by a factor of ~ 2 when considering the higher sensitivity JWST data, finding a bar fraction of 20 per cent at $z \sim 1$–2. At $z \sim 2$–3, the bar fraction drops to 15 per cent. As shown in Fig. 4, these trends are reproduced in the Auriga simulations, with a decreasing fraction of barred galaxies as a function of redshift. It is important to note that our sample covers a small mass range at $z = 0$, and therefore our results do not make predictions for the behaviour of lower mass galaxies.

Cosmological simulations with different galaxy formation models do not all agree on the bar fraction at low and high redshifts. For example, some studies find a dearth of bars at high redshifts, which is exacerbated at low redshifts (e.g. Reddish et al. 2022). Other studies of bar fractions using 'big box' cosmological simulations (e.g. Peschken & Łokas 2019; Gargiulo et al. 2022; Rosas-Guevara et al. 2022) find a flat, or rising bar fraction from $z = 0$ to $z \sim 1$, in contrast to most observational studies of bar fractions which find a decreasing bar fraction. One possible explanation for this mismatch (as mentioned in the latter studies) is that observational studies are not able to find short bars at higher redshifts, due to resolution limits. However, another possible explanation for this mismatch could be that the galaxy formation models employed affect the bar fraction across redshift. Whether the bar fraction remains flat/rising or decreases towards higher redshifts will therefore be an important point to settle in upcoming observational studies with higher spatial resolution and sensitivity, for example by using data from facilities such as JWST.

In the mass range probed by our simulations, we find that bars that form at higher redshifts tend to form longer than their local Universe counterparts. This occurs because bars at high redshifts tend to be triggered by interactions and/or mergers, which might cause the bars to form more 'saturated', i.e. longer. As shown in Fig. 9 this results in

these galaxies having a higher ratio of bar length relative to the disc size, as compared to local galaxies. Therefore – for stellar masses in the range probed by our sample – we might expect to find that observed high redshift bars (e.g. with JWST) are relatively long, and that the bar length-to-disc size ratio is larger than that observed in the local Universe.

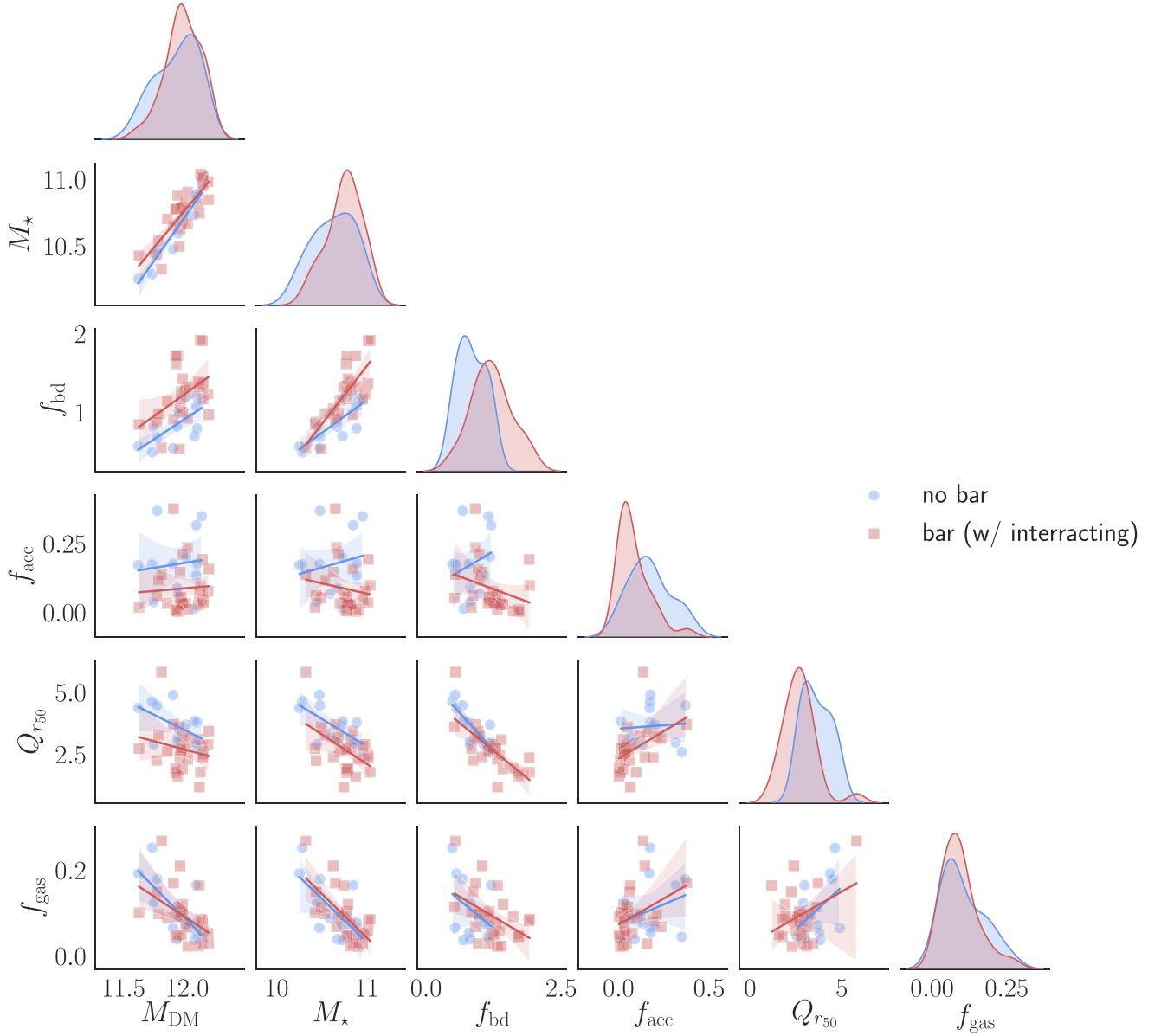### 5.3 The multiparameter space of bar formation

In this work, we have explored various galaxy properties which are thought to affect bar formation, in order to gain a better understanding of the role these parameters play when taken into account within the global cosmological context. This can help pave the way towards establishing the multiparameter space that sets whether a galaxy will form a bar or not within the cosmological setting, which could have a number of useful applications (e.g. for determining whether a galaxy will form a bar in semi-analytic cosmological simulations).

We attempt to summarize our findings in Fig. 18, where we show the distribution of barred and unbarred galaxies in different combinations of the parameter space we have explored in the previous sections. We find that, as discussed, the main parameters that separate out the barred-unbarred population are mainly the baryon-dominance f_{bd}, the fraction of accreted stars within the inner region (bulge) of the galaxy f_{acc} and the Toomre Q parameter of the inner galaxy $Q_{r_{50}}$, although we note that there is significant overlap between in which galaxy will be barred or unbarred in either one of these properties separately. However, for some of properties, for example the gas fraction f_{gas} or the dark matter halo mass M_{DM}, the barred and unbarred samples are completely overlapping. In future, this multidimensional parameter space could be used to build a semi-empirical model for bar formation within the cosmological context.

6 SUMMARY AND CONCLUSIONS

In this work, we study the formation and evolution of barred galaxies in the cosmological context, using the Auriga suite of cosmological zoom-in simulations, focusing on galaxies around the mass of the Milky Way (i.e. with halo masses between $0.5 \times 10^{12} - 2 \times 10^{12} M_\odot$ at $z = 0$). We start by exploring the properties of barred galaxies and

Figure 18. The multidimensional parameter space of bar formation: dark matter halo mass (M_{DM}), stellar mass ($M_\star$), baryon-dominance (f_{bd}), fraction of accreted stars in the central bulge regions (f_{acc}), the Toomre parameter within the half-mass radius ($Q_{r_{50}}$) and the gas fraction (f_{gas}), all at $z = 0$. The red (blue) points indicate the barred (unbarred) sample, including interacting galaxies. We see that the barred-unbarred populations separate out for the baryon dominance, accreted bulge fraction and Toomre Q parameters.

how these evolve over cosmic history. We then focus our attention on the question 'which galaxies form bars?' – i.e. we examine the various galaxy properties which are thought to play a role in the formation of bars. This enables us to determine the importance of these various properties within the cosmological context, in order to begin piecing together the multidimensional parameter space that drives bar formation. We summarize our results below.

In terms of the global properties of barred galaxies and on the evolution of bars, we find that:

(i) In Auriga, the fraction of barred galaxies decreases up to $z \sim 1$, and then remains ~ 20 per cent out to $z \sim 3$, consistent with the observed bar fraction found from recent JWST studies (Fig. 4). The

fraction of barred galaxies is higher in high-mass galaxies across the redshifts explored.

(ii) Below $z \sim 2$, bars in the Auriga simulations are robust, long-lived structures. They have a wide range of formation times, with the oldest bar in our sample forming at lookback time of $t_{lb} = 10.37$ Gyr and the youngest forming at $t_{lb} = 0.34$ Gyr (e.g. Fig. 3).

(iii) At $z = 0$, older bars tend to also be stronger, although with significant scatter in the relation (Fig. 5).

(iv) The bar formation time, t_{bf}, correlates with (i) the time at which the galaxy becomes baryon-dominated, (ii) the time at which the galaxy assembles 50 per cent of its stellar mass, as well as with (iii) the baryon-dominance of the galaxy at $z = 0$; it does not correlate with the host galaxy's stellar mass $M_\star$ at $z = 0$ (e.g. Figs 5 and 6).

(v) Bars that form at higher redshifts in our simulations tend to be longer than those that form in the low redshift Universe (Fig. 8). We find that this is due to the fact that bars at high redshifts are formed just after a significant merger, which leads them to form with a saturated length (Fig. 7).

(vi) Barred galaxies at high redshifts have larger bar-to-disc size ratios, due to the fact that bars forming in the early Universe are longer and have smaller size stellar discs (Fig. 9).

When exploring the physical properties that are important for determining whether a galaxy will form a bar or not, we find the following:

(i) Baryon-dominance is confirmed to play a prominent role in determining whether a galaxy will form a bar or not, with barred galaxies being on average more baryon-dominated from high redshifts, down to $z = 0$. This leads to barred galaxies being offset from commonly used abundance matching relations (e.g. Moster et al. 2013) in the $M_\star - M_h$ plane (Figs 10 and 11).

(ii) Galaxies that form bars assemble their stellar mass more rapidly (on average ~ 3 Gyr earlier) than unbarred galaxies (Fig. 11).

(iii) Galaxies that are offset from the abundance matching relation – i.e. which are baryon-dominated – but which do not have a bar at $z = 0$, tend to have a higher fraction of accreted material in their bulge (Fig. 14). This suggests that galaxies with a larger *ex situ* bulge are more stable against bar formation. On average, barred galaxies have a lower *ex situ* bulge than unbarred galaxies at $z = 0$ (Fig. 13).

(iv) Unbarred galaxies tend to have a larger Toomre Q parameter, and therefore more stable discs, both at high redshifts (i.e. around the time of bar formation) and at $z = 0$ (Fig. 16).

(v) On average, unbarred galaxies have higher gas fractions than barred galaxies. However, when controlling for stellar mass, the difference between barred and unbarred galaxies in terms of gas fraction disappears (Fig. 15). This suggests that differences in gas fraction are a secondary effect which is due to differences in the stellar mass (coupled to the fact that bars are more common in high mass galaxies in our sample). For a given stellar mass and/or baryon-dominance, barred and unbarred galaxies have similar gas fractions. We therefore do not find that gas fraction plays a major role in itself, in whether or not a galaxy will be barred.

(vi) We summarize our results on the multidimensional parameter space that drives bar formation in Fig. 18, where we see that the barred and unbarred samples separate out best in baryon dominance (f_{bd}), accreted bulge fraction (f_{acc}) and Toomre Q parameter.

The fact that barred galaxies tend to be more baryon-dominated has important consequences for the loci of barred and unbarred galaxies in the TF relation (see Fig. 17). Namely, barred galaxies are offset from unbarred galaxies in the TF relation (i.e. for the same V_{flat}, barred galaxies have a larger $M_\star$ or $M_{baryonic}$). Confirming this offset for barred galaxies in the observed TF relation would have important implications for the existence of dark matter, since such an offset cannot be readily explained in a modified gravity (e.g. MOND) framework.

ACKNOWLEDGEMENTS

DATA AVAILABILITY

All the data used, as well as parts of the auxiliary data produced for this paper, are publicly available to download at https://wwwmpa.mpa-garching.mpg.de/auriga/data.html

REFERENCES

Abadi M. G., Navarro J. F., Steinmetz M., Eke V. R., 2003, ApJ, 597, 21
Abraham R. G., Merrifield M. R., Ellis R. S., Tanvir N. R., Brinchmann J., 1999, MNRAS, 308, 569
Aguerri J. A. L., Méndez-Abreu J., Corsini E. M., 2009, A&A, 495, 491
Algorry D. G. et al., 2017, MNRAS, 469, 1054
Amvrosiadis A., et al., 2025, MNRAS, 537, 1163
Ansar S., Pearson S., Sanderson R. E., Arora A., Hopkins P. F., Wetzel A., Cunningham E. C., Quinn J., 2025, ApJ, 978, 37
Athanassoula E., 1992, MNRAS, 259, 345
Athanassoula E., 2002, ApJ, 569, L83
Athanassoula E., 2003, MNRAS, 341, 1179
Athanassoula E., Misiriotis A., 2002, MNRAS, 330, 35
Athanassoula E., Sellwood J. A., 1986, MNRAS, 221, 213
Athanassoula E., Lambert J. C., Dehnen W., 2005, MNRAS, 363, 496
Athanassoula E., Machado R. E. G., Rodionov S. A., 2013, MNRAS, 429, 1949
Athanassoula E., Rodionov S. A., Prantzos N., 2017, MNRAS, 467, L46
Berentzen I., Shlosman I., Martinez-Valpuesta I., Heller C. H., 2007, ApJ, 666, 189
Bittner A. et al., 2020, A&A, 643, A65
Blázquez-Calero G., et al., 2020, MNRAS, 491, 1800
Bournaud F., Combes F., 2002, A&A, 392, 83
Bournaud F., Combes F., Semelin B., 2005, MNRAS, 364, L18
Bovy J., Rix H.-W., 2013, ApJ, 779, 115
Buck T., Ness M. K., Macciò A. V., Obreja A., Dutton A. A., 2018, ApJ, 861, 88
Chabrier G., 2003, PASP, 115, 763
Collier A., Shlosman I., Heller C., 2018, MNRAS, 476, 1331
Combes F., Sanders R. H., 1981, A&A, 96, 164
Combes F., Debbasch F., Friedli D., Pfenniger D., 1990, A&A, 233, 82
Comerón S., Knapen J. H., Beckman J. E., Laurikainen E., Salo H., Martínez-Valpuesta I., Buta R. J., 2010, MNRAS, 402, 2462
Costantin L. et al., 2023, Nature, 623, 499

Courteau S., Andersen D. R., Bershady M. A., MacArthur L. A., Rix H.-W., 2003, ApJ, 594, 208

Curtis H. D., 1918, Publications of Lick Observatory, 13, 9

Debattista V. P., Liddicott D. J., Khachaturyants T., Beraldo e Silva L., 2020, MNRAS, 498, 3334

Di Matteo P. et al., 2015, A&A, 577, A1

Efstathiou G., Lake G., Negroponte J., 1982, MNRAS, 199, 1069

Ellison S. L., Nair P., Patton D. R., Scudder J. M., Mendel J. T., Simard L., 2011, MNRAS, 416, 2182

Erwin P., 2005, MNRAS, 364, 283

Erwin P., 2018, MNRAS, 474, 5372

Eskridge P. B. et al., 2000, AJ, 119, 536

Finkelstein S. L. et al., 2023, ApJ, 946, L13

Fragkoudi F., Athanassoula E., Bosma A., Iannuzzi F., 2015, MNRAS, 450, 229

Fragkoudi F., Athanassoula E., Bosma A., 2016, MNRAS, 462, L41

Fragkoudi F., Athanassoula E., Bosma A., 2017a, MNRAS, 466, 474

Fragkoudi F., Di Matteo P., Haywood M., Gómez A., Combes F., Katz D., Semelin B., 2017b, A&A, 606, A47

Fragkoudi F., Di Matteo P., Haywood M., Khoperskov S., Gomez A., Schultheis M., Combes F., Semelin B., 2017c, A&A, 607, L4

Fragkoudi F., Di Matteo P., Haywood M., Schultheis M., Khoperskov S., Gómez A., Combes F., 2018, A&A, 616, A180

Fragkoudi F. et al., 2020, MNRAS, 494, 5936

Fragkoudi F., Grand R. J. J., Pakmor R., Springel V., White S. D. M., Marinacci F., Gomez F. A., Navarro J. F., 2021, A&A, 650, L16

Frankel N. et al., 2022, ApJ, 940, 61

Fujii M. S., Bédorf J., Baba J., Portegies Zwart S., 2018, MNRAS, 477, 1451

Gadotti D. A., 2009, MNRAS, 393, 1531

Gadotti D. A., 2011, MNRAS, 415, 3308

Gadotti D. A., Seidel M. K., Sánchez-Blázquez P., Falcón-Barroso J., Husemann B., Coelho P., Pérez I., 2015, A&A, 584, A90

Gadotti D. A. et al., 2019, MNRAS, 482, 506

Gargiulo I. D., et al., 2019, MNRAS, 489, 5742

Gargiulo I. D. et al., 2022, MNRAS, 512, 2537

Ghosh S., Di Matteo P., 2024, A&A, 683, A100

Grand R. J. J., et al., 2017, MNRAS, 467, 179

Grand R. J. J., et al., 2019, MNRAS, 490, 4786

Grand R. J. J., Fragkoudi F., Gómez F. A., Jenkins A., Marinacci F., Pakmor R., Springel V., 2024, MNRAS, 532,

Guo Y. et al., 2023, ApJ, 945, L10

Hasan H., Pfenniger D., Norman C., 1993, ApJ, 409, 91

Hilmi T. et al., 2020, MNRAS, 497, 933

Hohl F., 1971, ApJ, 168, 343

Hubble E. P., 1926, ApJ, 64, 321

Hubble E. P., 1936, Realm of the Nebulae. Yale University Press: New Haven

Irodotou D. et al., 2022, MNRAS, 513, 3768

Izquierdo-Villalba D. et al., 2022, MNRAS, 514, 1006

Jogee S. et al., 2004, ApJ, 615, L105

Knapen J. H., Pérez-Ramírez D., Laine S., 2002, MNRAS, 337, 808

Kormendy J., Kennicutt R. C., Jr, 2004, ARA&A, 42, 603

Kraljic K., Bournaud F., Martig M., 2012, ApJ, 757, 60

Kranz T., Slyz A., Rix H.-W., 2003, ApJ, 586, 143

Le Conte Z. A., et al., 2024, MNRAS, 530, 1984

Leaman R. et al., 2019, MNRAS, 488, 3904

Lelli F., McGaugh S. S., Schombert J. M., Desmond H., Katz H., 2019, MNRAS, 484, 3267

Lelli F., Di Teodoro E. M., Fraternali F., Man A. W. S., Zhang Z.-Y., De Breuck C., Davis T. A., Maiolino R., 2021, Science, 371, 713

Li X., Shlosman I., Pfenniger D., Heller C., 2023, MNRAS, 520, 1243

Łokas E. L., 2018, ApJ, 857, 6

Łokas E. L., 2019, A&A, 629, A52

López P. D., Scannapieco C., Cora S. A., Gargiulo I. D., 2024, MNRAS, 529, 979

de Lorenzo-Cáceres A. et al., 2019, MNRAS, 484, 5296

Lovell M. R. et al., 2018, MNRAS, 481, 1950

Lynden-Bell D., Kalnajs A. J., 1972, MNRAS, 157, 1

Marinacci F., Pakmor R., Springel V., 2014, MNRAS, 437, 1750

Marinacci F., Grand R. J. J., Pakmor R., Springel V., Gómez F. A., Frenk C. S., White S. D. M., 2017, MNRAS, 466, 3859

Martinez-Valpuesta I., Shlosman I., Heller C., 2006, ApJ, 637, 214

Masters K. L. et al., 2011, MNRAS, 411, 2026

McGaugh S. S., 2012, AJ, 143, 40

McGaugh S. S., Schombert J. M., Bothun G. D., de Blok W. J. G., 2000, ApJ, 533, L99

Melvin T. et al., 2014, MNRAS, 438, 2882

Méndez-Abreu J. et al., 2019, MNRAS, 482, L118

Menéndez-Delmestre K., Sheth K., Schinnerer E., Jarrett T. H., Scoville N. Z., 2007, ApJ, 657, 790

Merrow A., Grand R. J. J., Fragkoudi F., Martig M., 2024, MNRAS, 531, 1520

Milgrom M., 1983, ApJ, 270, 365

Mo H. J., Mao S., White S. D. M., 1998, MNRAS, 295, 319

Moster B. P., Naab T., White S. D. M., 2013, MNRAS, 428, 3121

Ness M. et al., 2013, MNRAS, 430, 836

Norman C. A., Sellwood J. A., Hasan H., 1996, ApJ, 462, 114

Oman K. A., Navarro J. F., Sales L. V., Fattahi A., Frenk C. S., Sawala T., Schaller M., White S. D. M., 2016, MNRAS, 460, 3610

Ormerod K. et al., 2024, MNRAS, 527, 6110

Ostriker J. P., Peebles P. J. E., 1973, ApJ, 186, 467

Pakmor R., Springel V., Bauer A., Mocz P., Munoz D. J., Ohlmann S. T., Schaal K., Zhu C., 2016, MNRAS, 455, 1134

Patsis P. A., Skokos C., Athanassoula E., 2002, MNRAS, 337, 578

Peschken N., Łokas E. L., 2019, MNRAS, 483, 2721

Petersen M. S., Weinberg M. D., Katz N., 2024, MNRAS, 531, 751

Pfenniger D., Friedli D., 1991, A&A, 252, 75

Planck CollaborationXVI, 2014, A&A, 571, A16

Ponomareva A. A., Verheijen M. A. W., Peletier R. F., Bosma A., 2017, MNRAS, 469, 2387

Portail M., Wegg C., Gerhard O., 2015, MNRAS, 450, L66

Posti L., Fall S. M., 2021, A&A, 649, A119

Posti L., Fraternali F., Marasco A., 2019, A&A, 626, A56

Power C., Navarro J. F., Jenkins A., Frenk C. S., White S. D. M., Springel V., Stadel J., Quinn T., 2003, MNRAS, 338, 14

Quillen A. C., Minchev I., Sharma S., Qin Y.-J., Di Matteo P., 2014, MNRAS, 437, 1284

Raha N., Sellwood J. A., James R. A., Kahn F. D., 1991, Nature, 352, 411

Reddish J. et al., 2022, MNRAS, 512, 160

Rizzo F., Vegetti S., Powell D., Fraternali F., McKean J. P., Stacey H. R., White S. D. M., 2020, Nature, 584, 201

Rosas-Guevara Y. et al., 2020, MNRAS, 491, 2547

Rosas-Guevara Y. et al., 2022, MNRAS, 512, 5339

Roshan M., Ghafourian N., Kashfi T., Banik I., Haslbauer M., Cuomo V., Famaey B., Kroupa P., 2021, MNRAS, 508, 926

de Sá-Freitas C. et al., 2023, A&A, 671, A8

Sackett P. D., 1997, ApJ, 483, 103

Saha K., Martinez-Valpuesta I., Gerhard O., 2012, MNRAS, 421, 333

Saha K., Gerhard O., Martinez-Valpuesta I., 2016, A&A, 588, A42

Sakai S. et al., 2000, ApJ, 529, 698

Scannapieco C., Athanassoula E., 2012, MNRAS, 425, L10

Sellwood J. A., 1980, A&A, 89, 296

Sellwood J. A., Gerhard O., 2020, MNRAS, 495, 3175

Sheth K., et al., 2008, ApJ, 675, 1141

Simmons B. D. et al., 2014, MNRAS, 445, 3466

Smail I. et al., 2023, ApJ, 958, 36

Sormani M. C., Sobacchi E., Fragkoudi F., Ridley M., Treß R. G., Glover S. C. O., Klessen R. S., 2018, MNRAS, 481, 2

Springel V., 2010, MNRAS, 401, 791

Toomre A., 1964, ApJ, 139, 1217

Tsukui T., Wisnioski E., Bland-Hawthorn J., Mai Y., Iguchi S., Baba J., Freeman K., 2024, MNRAS, 527, 8941

Tully R. B., Fisher J. R., 1977, A&A, 54, 661

Vogelsberger M., Genel S., Sijacki D., Torrey P., Springel V., Hernquist L., 2013, MNRAS, 436, 3031

Weiner B. J., Sellwood J. A., Williams T. B., 2001, ApJ, 546, 931

van der Wel A. et al., 2014, ApJ, 788, 28
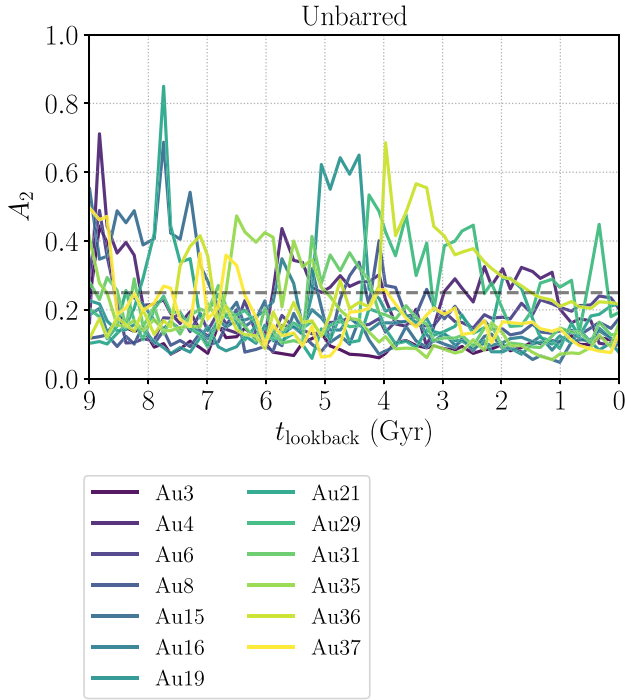
Figure A1. The $m = 2$ Fourier mode of the surface density as a function of lookback time for galaxies that are not classified as barred at $z = 0$.

APPENDIX A: THE EVOLUTION OF UNBARRED GALAXIES

In Fig. A1, we show the evolution of the bar strength A_2 as a function of redshift for the galaxies which do not contain a bar at $z = 0$ in our sample, in order to explore if any of these galaxies have at some point hosted a bar. We examine in detail the galaxies in this sample that have peaks or spikes in A_2, to explore whether these are indeed due to the presence of a bar. We find that in all but one of these galaxies, the peaks in A_2 are not due to the presence of a stellar bar, but are transient effects due to interactions and/or mergers. The exception to this rule is Au36 which does indeed form a bar at a $t_{lb} \sim 4\,\mathrm{Gyr}$, which is subsequently gradually weakened by an interaction. This leads to the dissolution of the bar in this galaxy, which appears as an unbarred (or very weakly barred) at $z = 0$ according to our definition (which requires $A_2 > 0.25$). We therefore see that in the Auriga simulations bars are long-lived structures, with only one case of a bar that is severely weakened after its formation.

## APPENDIX B: RELATION BETWEEN DIFFERENT ESTIMATES OF BARYON-DOMINANCE

In Fig. B1, we show the relation between the ratio of stellar to dark matter within 5 kpc (f_{bd}) versus the offset from the abundance
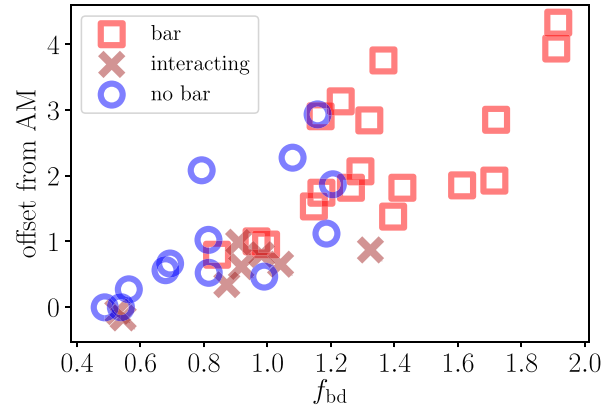

Figure B1. The relation between the ratio of stars to dark matter within 5 kpc (f_{bd}) versus the offset from the abundance matching relation ($\delta M_\star$). The two quantities are correlated.

matching relation of Moster et al. (2013) as defined in Section 4.1 by $\delta M_{\star,\mathrm{AM}}$. We see that the two are correlated. The baryon-dominance f_{bd} of the barred galaxies can also be seen in Fig. B2, where the circular velocity curves for the barred sample (left) and the unbarred sample (right) are plotted. Solid lines give the average values for the two samples and the shaded regions the 1σ dispersion. The thin black lines in both panels correspond to the MW14 model of Bovy & Rix (2013). We see that the barred population is more baryon-dominated, i.e. the stellar component dominates in the inner regions, and they are overall more massive (higher circular velocity). The vertical lines give the point at which the stellar and dark matter components cross each other, which for the MW14 model occurs around ~ 13.5 kpc. For the Auriga barred population it occurs around 8 kpc, while for the unbarred population it occurs at smaller radii (as expected for more dark matter dominated systems) at around 4 kpc. We see that even though barred galaxies in Auriga are more baryon-dominated than unbarred ones, they are not as baryon-dominated as dynamical models for the Milky Way predict.

In Fig. B3, we show the baryon-dominance within the half-mass radius (r_{50}) as a function of time, for the barred and unbarred populations (solid line shows the average and the shaded region shows the 1σ dispersion). This shows a similar trend to that discussed in Fig. 11, i.e. we find that barred galaxies are more baryon-dominated at earlier times than unbarred galaxies. Unbarred galaxies on the other hand stay dark matter dominated within the inner regions even down to $z = 0$, within the half-mass radius.
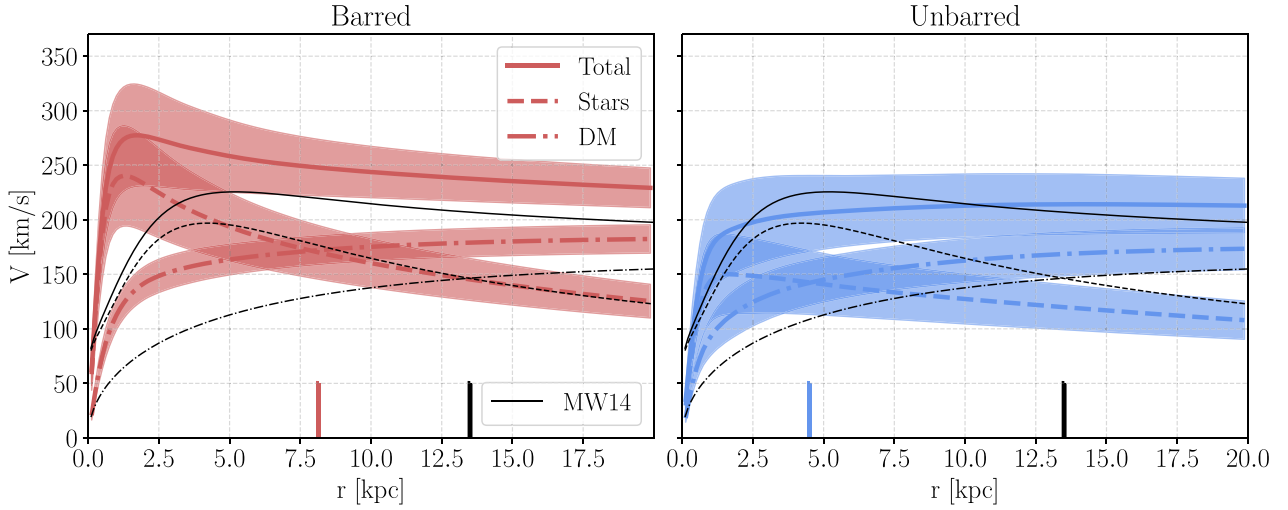
Figure B2. Rotation curve of barred (left) and unbarred (right) galaxies in the Auriga simulation. We show the mean and 1σ dispersion for the total (solid), stars (dashed), and dark matter (dot–dashed). The contribution to circular velocity from the gas is not shown here but is included in $V_{\rm tot}$. The MW14 model is shown in black. The radius at which the dark matter begins to dominate over the stars is shown as vertical arrows on the bottom x-axis for the Auriga galaxies (red and blue) and the MW14 model (black).
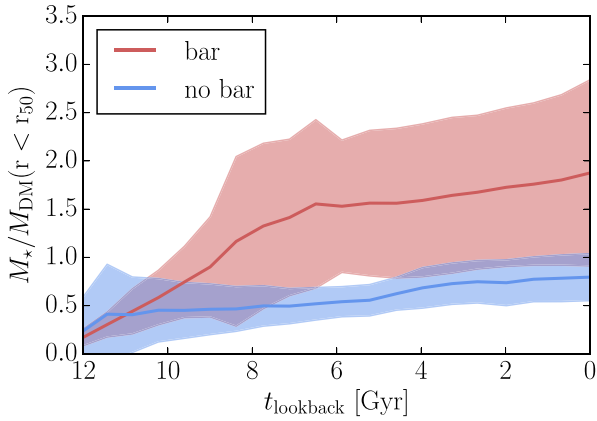

Figure B3. The average (solid lines) and standard deviation (shaded regions) of the ratio of stellar-to-dark matter mass within the half-mass radius as a function of time for the barred galaxies (excluding the interacting galaxies), in red, and for the unbarred galaxies, in blue. On average, for barred galaxies, the stellar mass dominates over the dark matter mass within the half-mass radius by $z \sim 0$, in contrast to unbarred galaxies which tend to be more dark matter dominated over all cosmic times.

APPENDIX C: THE BARYONIC TF RELATION

Here, we extend our discussion in Section 5.1 to the baryonic TF Relation. Studies have shown that using the total baryonic mass of galaxies, i.e. combining both the gaseous and stellar component, results in even less intrinsic scatter in the relation, which is referred to as the Baryonic TF relation (BTFR; e.g. McGaugh et al. 2000). The BTFR has less than 0.05 dex in orthogonal intrinsic scatter and ~ 0.075 dex in vertical scatter (Lelli et al. 2019).

In the left panel of Fig. C1, we explore the BTFR for barred (excluding interacting) and unbarred galaxies in our sample. To obtain the baryon mass we add the gas mass of the galaxy – which we obtain by summing all the gas within $0.1r_{200}$ and $z < 2$ kpc – to the stellar mass. In this mass regime the gas fractions are quite low (below 10 per cent for most galaxies) and as such, the results are similar to those found for the STFR, i.e. the barred galaxies are on average slightly offset from the unbarred galaxies, although the offset is less pronounced. We also find that the slope is decreased for the BTFR, i.e. we find a slope of ~ 3, as opposed to the STFR where we found a slope of ~ 3.6 (see Section 5.1). We note that it is not uncommon to find shallower slopes for samples that focus only on the high mass regime (see e.g. Oman et al. 2016).
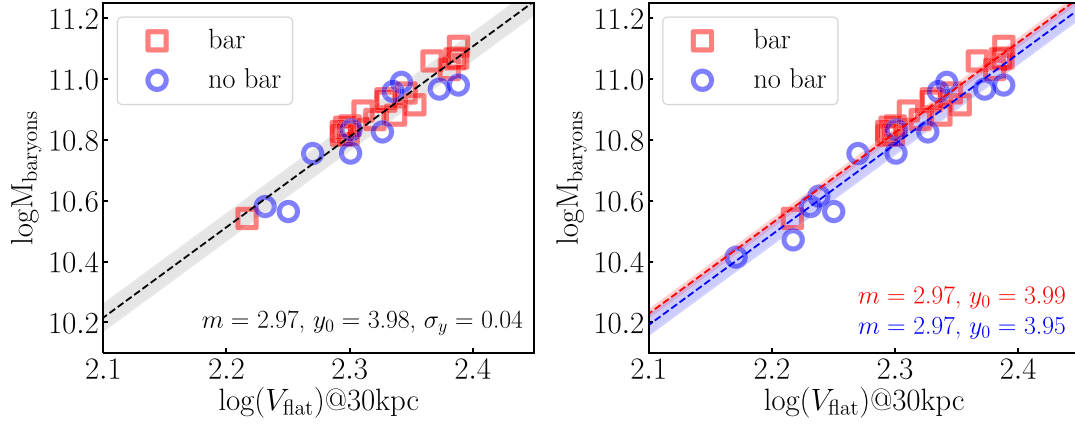
Figure C1. The Baryonic TF relation for galaxies at $z = 0$ in Auriga. *Left*: The grey dot–dashed line shows the relation given by fitting all galaxies together, while the shaded region indicates the intrinsic scatter σ_y. *Right*: The red (blue) dashed line shows the relation when fitting only the barred (unbarred) galaxies. The shaded regions indicate the uncertainties from boostrapping (see the text). The scatter is slightly reduced for the BTFR as compared to the STFR and the barred and unbarred BTFR relations are less separated.

This paper has been typeset from a TEX/LATEX file prepared by the author.